Chemical Kinetics of SCRAMJET Propulsion

by

Rodger Joseph Biasca

S.B. Aeronautics and Astronautics, Massachusetts Institute of Technology, 1987

SUBMITTED IN PARTIAL FULFILLMENT OF THE
REQUIREMENTS FOR THE DEGREE OF

Master of Science

in

Aeronautics and Astronautics

at the

Massachusetts Institute of Technology

July 1988

Signature of Author _____

Department of Aeronautics and Astronautics
July 1988

Certified by _____

Professor Jean F. Louis, Co- Thesis Supervisor
Department of Aeronautics and Astronautics

Professor Manuel Martinez-Sanchez, Co- Thesis Supervisor
Department of Aeronautics and Astronautics

Dr. Phillip D. Hattis, Technical Supervisor
s Stark Draper Laboratory

Accepted by _____

Professor Harold Y. Wachman, Chairman
Department Graduate Committee

Chemical Kinetics of SCRAMJET Propulsion

by

Rodger Joseph Biasca

Submitted to the Department of
Aeronautics and Astronautics
in partial fulfillment of the
requirements for the degree of
Master of Science in Aeronautics and Astronautics

Recent interest in hypersonics has focused on the development of a single stage to orbit vehicle propelled by hydrogen fueled SCRAMJETs. Necessary for the design of such a vehicle is a thorough understanding of the chemical kinetic mechanism of hydrogen-air combustion and the possible effect this mechanism may have on the performance of the SCRAMJET propulsion system. This thesis investigates possible operational limits placed on a SCRAMJET powered vehicle by the chemical kinetics of the combustion mechanism and estimates the performance losses associated with chemical kinetic effects. The investigation is carried out through the numerical solution of one dimensional fluid flow equations coupled with the chemical kinetic expressions for the time rate of change of the fluid composition.

The results of the investigation show the hydrogen-air combustion process will place limitations on the pressure and temperature that must be maintained at the combustor entrance. For low initial pressures ($P < 0.5$ atm) and temperatures ($T < 1000$ K), the reactions become too slow for total heat release to be realized within a reasonable combustor length. In addition, hydrogen may fail to ignite for temperatures below 1000 K. Using a control volume method, it is shown that these required temperatures and pressures cannot be maintained over the entire trajectory for a vehicle with a fixed geometry.

In addition to the heat release problems, low pressures lead to substantial losses in nozzle performance. Low pressures mean third body reactions, the main path for recombination of free radicals, are inefficient. The dissociation energy in the flow exiting the combustor cannot be converted into kinetic energy in the nozzle. The nozzle freezes, leading to a drop in performance.

Finally, the specific impulse of the vehicle is shown to drop dramatically with decreasing combustor pressure. Best vehicle performance is achieved for flight at altitudes below the trajectories usually associated with hypersonic vehicles.

Thesis Co-supervisors: Jean F. Louis
Professor of Aeronautics and Astronautics

Manuel Martinez-Sanchez
Associate Professor of Aeronautics and Astronautics

Acknowledgements

Several days before the completion of this thesis, the life of Professor Jean Louis was tragically claimed in an auto accident. I dedicate this thesis to Professor Louis, whose guidance and encouragement have been so invaluable. The loss of Professor Louis is the loss of a good advisor and friend.

Many others have provided assistance in the course of writing this thesis. On this page, I only briefly mention a few and hope everyone understands my gratitude is more than can be expressed here. In particular, I would like to thank Professor Martinez-Sanchez, who has provided much of the direction of this thesis. Also, I owe a special debt of gratitude to Phil Hattis and Draper Laboratory for the foresight and financial support to pursue the topic of the once-again-fashionable hypersonic vehicle. On a more personal note, Mark Lewis, in addition to just being a good friend over the last year and a half, has provided a great deal of advice during my work on this thesis. Finally, I must thank my parents for 24 years of support and love.

[0]This thesis was written under IR&D Task 236 of the Charles Stark Draper Laboratory, Inc. Publication of this thesis does not constitute approval by The Charles Stark Draper Laboratory, Inc. of the findings or conclusions contained herein.

Contents

Acknowledgements 1

1 Introduction 7

1.1 General Vehicle Configuration 7

1.2 Chemistry Models for SCRAMJET Analysis 8

1.3 Thesis Goals 11

2 Analysis 12

2.1 Inlet 12

2.2 Quasi-One Dimensional Flow Equations 14

2.3 Finite Rate Chemistry 17

2.4 Equilibrium Flow 19

2.5 Numerical Solution 26

3 Inlet Results 28

4 Static Reaction Results 32

4.0.1 Hydrogen-Air System 32

4.0.2 Hydrogen-Air-Hydrogen Peroxide System 38

4.0.3 Hydrogen-Air-Silane System 38

5 Nozzle Results 45

6 Vehicle Performance Results 57

7 Conclusions 66

A Thermodynamic and Reaction Rate Data 71

List of Figures

1.1 General Configuration of a Hypersonic Vehicle. 8

2.1 Inlet at design conditions. 13
2.2 Inlet below design conditions. 13
2.3 Inlet above design conditions. 13
2.4 Model of the quasi-one-dimensional fluid element. 15

3.1 Pressure and temperature delivered to the combustor for the first design point. 29
3.2 Residence time per meter of a fluid element in the combustor assuming constant velocity (first design point). 29
3.3 Pressure and temperature of the flow delivered to the combustor for the second design point. 30
3.4 Residence time per meter in the combustor for the second design point. 30

4.1 Time history of the mass fractions in a stoichiometric hydrogen-air reaction with an initial temperature of 1000 K and an initial pressure of 1 atm. . . 34
4.2 Time history of the temperature in a stoichiometric hydrogen-air reaction with an initial temperature of 1000 K and an initial pressure of 1 atm. . . 34
4.3 Total reaction times for the H_2-Air system as a function of initial temperature and pressure. 35
4.4 Effect of equivalence ratio on the H_2-Air reaction. 36
4.5 Required lengths of the combustor at the first design point for complete combustion to occur. 37
4.6 Required lengths of the combustor at the second design point for complete combustion to occur. 37
4.7 Total reaction times for the H2-air-2.5% H_2O_2 system as a function of initial temperature and pressure 39

4.8 The effect of increased mass fraction of H_2O_2 on the total reaction time for various initial temperatures and pressure 39
4.9 Effect of hydrogen peroxide as a function of temperature for T<1050 K . 40
4.10 Total reaction times for the H_2-Air-2.5% mass fraction SiH_4 system as a function of initial temperature and pressure. 41
4.11 Effect of increasing SiH_4 on the reaction time. 41
4.12 Total reaction times for mixtures containing 5% and 10% mass fraction silane as a function of temperature and pressure 42
4.13 The effect of 5% silane on the lengths required for total combustion. Design point 1 43
4.14 The effect of 5% silane on the lengths required for total combustion. Design point 2. 44
4.15 The effect of 10% silane on the lengths required for total combustion. Design point 2 44

5.1 ϕ vs initial pressure and temperature for an initial velocity of 5500 m/s and 12.5 degree half angle conical expansion 46
5.2 τ as a function of pressure and temperature for an initial velocity of 5500 m/s 46
5.3 ζ as a function of pressure and temperature for an initial velocity of 5500 m/s 47
5.4 Effect of velocity on ϕ. 49
5.5 Effect of velocity on τ. 49
5.6 Effect of velocity on ζ. 50
5.7 Effect of area ratio on ϕ. 52
5.8 The effect of area ratio on τ. 52
5.9 The effect of area ratio on ζ. 53
5.10 The effect of nozzle half angle on ϕ. 55
5.11 The effect of nozzle half angle on τ. 55
5.12 The effect of nozzle half angle on ζ. 56

6.1 Specific impulse vs. Mach number and altitude for the first design point. 59
6.2 Specific impulse vs. Mach number and altitude for the second design point. 59
6.3 Penalty for kinetic solution for first design point. 61
6.4 Penalty if nozzle were completely frozen for second design point. 61
6.5 Penalty for kinetic solution for second design point. 62

6.6 Penalty if nozzle were completely frozen for first design point. 62
6.7 Specific impulse vs. equivalance ratio for various flight conditions. Design point 1. 63
6.8 Specific impulse vs. equivalance ratio for various flight conditions. Design point 2. 63

List of Tables

2.1 Influence Coefficients with Chemistry Added: Fuel and Area. 20
2.2 Influence Coefficients with Chemistry Added: Fuel and Pressure. 20
2.3 Influence Coefficients with Chemistry Added: Fuel and Temperature. . . 20

5.1 Numbering system of lines 48

A.1 Polynomial curvefit coefficients for the enthalpy of individual chemical species in thermal equilibrium as a function of temperature 72
A.2 Polynomial curvefit coefficients for the enthalpy of individual chemical species in thermal equilibrium as a function of temperature (con't). 73
A.3 Reaction mechanism for the H_2-Air system and values of the constants for the Arrenhius expression. 74
A.4 Third body efficiency factors for the H_2-air system. 75
A.5 Silane reaction mechanism and values of the Arrenhius expression constants. 76

Chapter 1

Introduction

In 1986 a new national effort began to develop a hypersonic aircraft: interest in hypersonics is once again growing after having lain nearly dormant since the cancellation of the X-15 project in 1968.

Several possible missions exist for such a hypersonic aircraft. The aircraft considered here is a single stage to orbit vehicle capable of horizontal take- off and landing and propelled throughout the flight exclusively by air- breathing engines.

1.1 General Vehicle Configuration

Figure 1.1 shows the general configuration of the hypersonic vehicle most prevalent in the current literature (see for example References [1], [2] and [3]). Since no single air-breathing propulsion system is capable of providing efficient thrust across the entire trajectory from take-off (Mach number, M=0) to orbital velocity (M=25), the airbreathing engines must actually consist of several propulsive modes. From takeoff to M=3, conventional turbojets provide efficient thrust. Above approximately M=3, however, the efficiency of the turbojet begins to drop as large total pressure losses are accrued in the turbomachinery. Such components as the compressor must be removed from the flow path.

With the turbomachinery removed from the flow path, the engine becomes a ramjet. In the ramjet, a series of shocks compresses the incoming flow to subsonic velocities. Fuel is then combusted in the subsonic stream, and the flow re-expanded through a nozzle.

Above Mach 6, the shocks required to decelerate the flow to a subsonic velocity become quite strong, again causing large total pressure losses. For high Mach numbers, the flow is not decelerated to subsonic velocities. Instead, the fuel is combusted in a supersonic airstream. The engine becomes a supersonic combustion ramjet, or SCRAMJET.

Although the turbojet and ramjet propulsive modes are integral to the vehicles overall

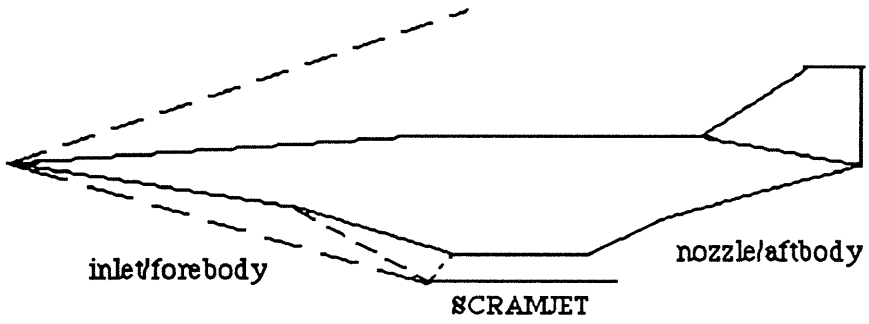

Figure 1.1: General Configuration of a Hypersonic Vehicle. The entire undersurface of the aircraft is integral to the propulsion system with the forebody acting as an inlet and the aftbody playing the role of a nozzle.

performance along the trajectory, the concern of this thesis is strictly limited to the chemical kinetic processes occurring in the SCRAMJET. With this in mind, the turbojet and ramjet modes will not be discussed further.

The figure shows the vehicle in the SCRAMJET propulsion mode. In this configuration, in order to increase thrust to weight ratios, the entire undersurface of the vehicle is integrated into the propulsion system. The forebody of the aircraft also acts as the engine inlet by providing a series of ramps to generate oblique shocks through which the incoming air is compressed. The compressed flow then enters the SCRAMJETs which act as the combustion chamber for the overall engine. Finally, the flow re-expands across the aftbody of the aircraft, which acts as the nozzle.

1.2 Chemistry Models for SCRAMJET Analysis

A single stage to orbit vehicle will encounter vastly varying flight regimes over its trajectory. Unfortunately, many of the conditions to be encountered are outside the range of conventional wind tunnel facilities. Without the conventional tool of the wind tunnel test, the aircraft's designers will need to rely heavily on computational fluid dynamics (CFD) to provide the analysis necessary for design.

In order to provide true performance estimates, the CFD codes need to solve the full 3-D Navier-Stokes equations. Integral to the success of these calculations is also the use of an accurate chemistry model. Unfortunately, even with the largest computers, calculations incorporating the most accurate (and most complex) chemistry models are presently

computationally and economically prohibitive. In addition, such solutions cannot easily be generalized to provide physical insight into the mechanisms affecting the performance of the vehicle. For preliminary designs, however, the calculations can be greatly simplified by hypothesizing simplified chemical models that adequately reproduce the true chemical effects.

Several chemical models of varying levels of complexity can be constructed:

- Perfect Gas

  In this model, the flow consists of a hypothetical perfect gas of constant composition and specific heat. Although quite simple, the model is inappropriate for situations above approximately 1200 K for air. Above this temperature, dissociation of oxygen changes both the chemical composition and specific heat of the gas. In addition, the model is obviously not suitable for combustion calculations where changing composition is the most important consideration.

- Frozen Gas

  Here, the composition of the gas is constant, but the specific heat varies as a function of temperature. Although an improvement over the perfect gas model in some situations, the frozen gas model is still limited to situations where the chemical composition of the gas is slowly varying.

- Equilibrium Gas

  In this model, the flow is assumed to be in chemical equilibrium at every point in the flow. This assumption allows the chemical composition of the flow to be determined from other thermodynamic variables such as pressure and temperature. Unfortunately, the determination of the chemical composition requires solving a set of nonlinear algebraic equations, a task that greatly increases the cost of computation over the previous models. In some situations, however, the equilibrium assumption can provide an adequate model of combustion without the additional complications introduced by the finite rate case discussed below. The equilibrium model fails when the characteristic times associated with the chemical reactions become of the same order as the characteristic time of the flow properties.

- Finite rate chemistry

  Finite rate chemistry models integrate the expressions for the time rate of change of the chemical composition of the gas. Although providing "real" estimates of

the chemistry that is occurring, the model introduces widely varying times scales into the problem, i.e. the governing equations become quite stiff. The stiffness of the equations requires sophisticated techniques for efficient integration. Even then, integration of complete reaction mechanisms taxes the largest computers.

Since the integration of the stiff equations again reaches the point of being computationally prohibitive, a subclass of "two step global reaction models" has been developed. As an example, for the combustion of H_2 in air, the complete reaction mechanism consists of approximately 60 reactions among 20 species. Many of these reactions and species are unimportant and can be ignored with negligible error. In the two step global model, the reaction mechanism is replaced by two hypothetical reaction paths among five species. The accurate reproduction of the true chemistry then requires the determination of the hypothetical reaction rates over a desired range of temperature and pressure. Several of these models have been developed in the literature.

- Finite rate chemistry with multiple modes of nonequilibrium

  The models above have only considered chemical nonequilibrium. However, in some situations, rotational and vibrational nonequilibrium may also exist. For the most accurate calculations, these modes should also be included in the rate calculations. Since further time scales are introduced, these calculations are usually beyond the capability of even the most sophisticated computer systems. Fortunately, however, since the characteristic relaxation times for the rotational and vibrational modes are usually much faster than the chemical time scales involved, equilibrium assumptions are usually adequate.

Most CFD codes presently in use for combustion calculations use either an equilibrium assumption or a two-step global reaction mechanism. Before applying these models, however, the designer must have a reasonable concept of the effect the assumption may have on the final solution.

1.3 Thesis Goals

The purpose of this thesis is to investigate the effect of finite rate chemistry on a SCRAM-JET. The investigation includes

- predicting operational limits of the vehicle dictated by the kinetics of the combustion process, and
- estimating the performance losses incurred from the chemistry.

In order to evaluate the effect of finite rate chemistry, the complete reaction mechanism must be considered. As mentioned above, a three- or even two- dimensional solution with the complete reaction mechanism requires extensive computing facilities. In order to retain the full reaction mechanism, this thesis will only consider quasi-one-dimensional flow. The restriction to quasi-one- dimension reduces the partial differential equations to ordinary differential equations, a great simplification since efficient methods exist to integrate large sets of coupled, stiff ODEs. Although clearly not quantitatively correct in areas of complicated geometry, the model does provide insight into the effects of the finite rate chemistry and shows where simpler models may be inadequate.

In keeping with the simplicity of the quasi-one-dimension assumption, and in order to retain the emphasis on the effects of the chemical kinetics, several other major effects will be ignored. The major further assumptions are that

- the flow is inviscid,
- heat losses are negligible,
- the fuel mixes instantaneously with the core flow in the engine.

The thesis is divided into seven chapters. Chapter 2 develops the analytic models of equilibrium and finite rate flow. In addition, a model of the inlet is included that is used to relate the combustor properties to the freestream flight conditions. The results of this inlet model are discussed in Chapter 3. Chapter 4 states the results of a static chemistry model. The static reaction model provides a way of easily investigating the operational limits placed on the vehicle by the combustion process. Chapter 5 presents the results for the vehicle nozzle and discusses the performance losses incurred from freezing in the nozzle. Chapter 6 presents the overall performance estimates of the propulsion system. Chapter 7 states the conclusions of the study.

Chapter 2

Analysis

The first section of this chapter develops a control volume method for the analysis of the engine inlet. Although the main focus of the thesis is the combustor and nozzle, the inlet analysis is required so the freestream flight conditions may be related to the initial conditions of the combustor/nozzle analysis. Following the inlet analysis, the governing equations for quasi-one-dimensional flow are stated, and the equations of the finite rate chemistry model derived. A section is also devoted to discussing the solution for equilibrium flow. The equilibrium flow solution is useful for comparative purposes with the finite rate case. The chapter concludes with short discussions on the numerical techniques used to integrate the equations.

2.1 Inlet

In order to relate the conditions at the beginning of the combustor to the freestream flight conditions, a model is needed for the inlet. For this thesis, the inlet consists of two ramps of equal turning angle. Figure 2.1 shows the general configuration of the inlet at the design conditions. At design, the shocks generated from the forward ramps intersect at the cowl lip. The cowl lip then reflects the shocks which are cancelled at the upper wall. A settling duct damps nonuniformities before the flow reaches the beginning of the combustor.

For a given design Mach number and ramp angle, the requirement that the shocks intersect at the cowl lip and are cancelled at the upper wall completely determines the geometry of the inlet. For flight off the design condition, the shocks no longer reflect from the cowl at the correct angle to be cancelled at the upper wall. As the vehicle moves below the design Mach number, the shocks move forward, missing the cowl (see Figure 2.2). At Mach numbers above the design condition (see Figure 2.3), the shocks intersect before reaching the cowl. They then enter the settling duct and weaken through a series

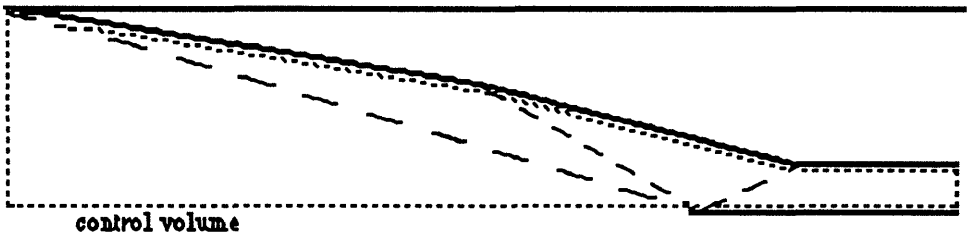

Figure 2.1: Inlet at design conditions. The shocks intersect at the cowl lip and are cancelled at the upper wall.

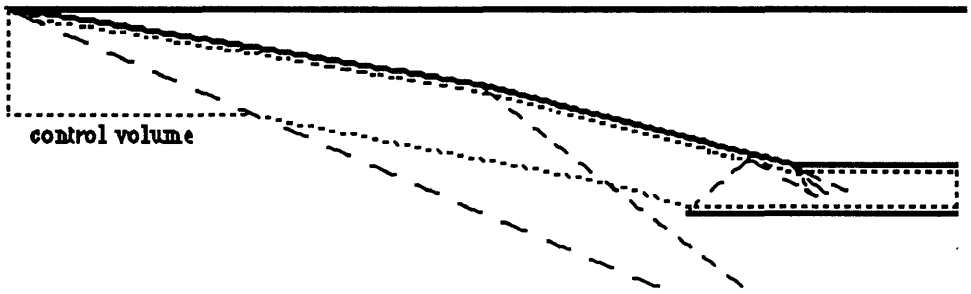

Figure 2.2: Inlet below design conditions. The shocks move forward missing the cowl lip. The shock generated from the cowl then intersects the upper wall, reflects, and begins a series of interactions with an expansion fan.

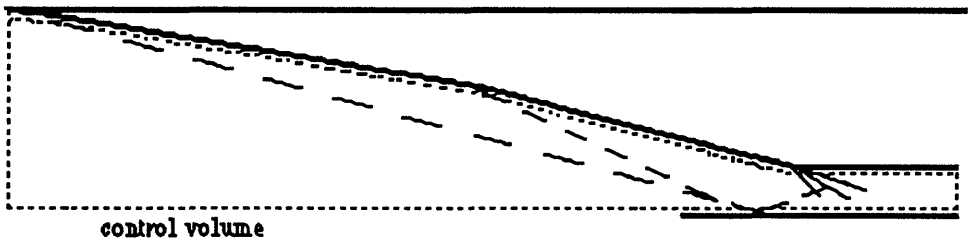

Figure 2.3: Inlet above design conditions. The shocks intersect before reaching the cowl, reflect from the cowl, and begin a series of interactions with the expansion fan.

of reflections.

With the geometry of the inlet determined for a given design Mach number and ramp angle, the global conservation equations can be solved to find the values of the flow properties at the beginning of the combustor. Denoting freestream conditions by the subscript '0' and conditions at the beginning of the combustor by the subscript 'e', the conservation equations for the control volumes shown in Figures 2.1 to 2.3 are

- Mass

$$\rho_0 u_0 A_0 = \rho_e u_e A_e \tag{2.1}$$

- Momentum

$$\rho_0 u_0 A_0 (u_e - u_0) = \sum_i P_i A_i \cos\theta_i \tag{2.2}$$

  where the summation is taken over the sides of the control volume and θ_i is the local inclination of the wall to the freestream velocity vector.

- Energy

$$h_0 + u_0^2/2 = h_e + u_e^2/2 \tag{2.3}$$

- State

$$P = \rho R T \tag{2.4}$$

The assumption is made that the gas is in equilibrium at point e. The enthalpy of the gas is then a function of pressure and temperature (the solution of the equilibrium composition is discussed in Section 2.4). Since the geometry is known from the design conditions, global conservation provides four equations for the four unknowns (ρ_e, u_e, P_e, T_e) at the combustor entrance. The solution of these four equations provides the conditions at the combustor entrance for any flight conditions.

2.2 Quasi-One Dimensional Flow Equations

This sections develops the equations of quasi-one-dimensional flow. The development follows closely the classical 'Influence Coefficient' method derived by Shapiro [4]. Figure 2.4 shows a differential element of gas of length dx travelling at a velocity, V, in the x-direction along a channel of cross sectional height, A. The fluid properties of interest are the pressure, P, temperature, T, density, ρ, enthalpy, h, and molecular weight, w. The fuel fraction, f, is defined as

$$\dot{m} = \dot{m}_0 (1 + f). \tag{2.5}$$

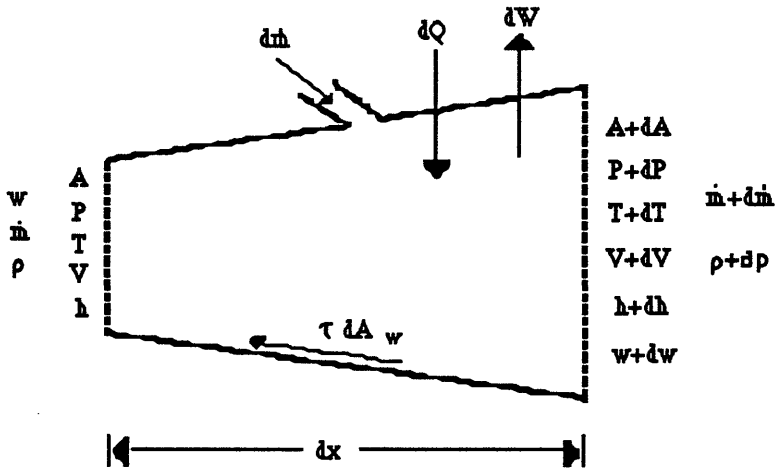

Figure 2.4: Model of the quasi-one-dimensional fluid element showing the change in fluid properties in the x-direction.

Mass is being injected into the stream at rate $\dot{m}_0\, df$, energy is being added at a rate of dQ, and work is being done on external bodies at rate dW. In addition, a frictional force given by $\tau_w\, dA_w$, where τ_w is the shear stress and dA_w is the wetted surface area of the differential element acts on the fluid.

For this element of fluid, the governing equations in differential form for quasi-one dimensional flow are

- State:

$$\frac{dP}{P} = \frac{d\rho}{\rho} + \frac{dw}{w} + \frac{dT}{T} \tag{2.6}$$

- Continuity:

$$\frac{df}{1+f} = \frac{d\rho}{\rho} + \frac{dA}{A} + \frac{dV}{V} \tag{2.7}$$

- Momentum:

$$\frac{dP}{\rho V^2} + \frac{dV}{V} + C_f \frac{dA_w}{2A} + \frac{df}{1+f} = 0 \tag{2.8}$$

- Energy:

$$dQ - dW = dh + V\, dV + h_T \frac{df}{1+f} \tag{2.9}$$

where the shear stress τ_w has been expressed in terms of the friction coefficient, C_f. Also, the term h_T represents the change in the total enthalpy of the injected gas between the wall temperature and the flow temperature, i.e. $h_T = (h + V^2/2)_T - (h + V^2/2)_{wall}$.

To find expressions for h and w, the fluid is considered to be a mixture of gases containing n_s molecular species, each of σ_j moles per kilogram flow. In addition, the

individual species are assumed to be in thermal equilibrium. (For justification of this assumption, the reader is referred to Vincenti and Kruger[5], where it is shown that rotational equilibrium will be reached within a few mean free paths of a strong shock. Comparison of the Landau-Teller model also shows the relaxation time for vibrational equilibrium to be much shorter than the chemical relaxation times for the gas of interest. Further information about the relaxation times for vibration can be found in the paper by Bussing [6].)

For individual chemical species in thermal equilibrium, the enthalpy must be a function of temperature alone, i.e. $h = h(T)$ [7]. The enthalpy as a function of temperature may be found from either the partition function or, more practically, polynomial curvefits derived from the partition functions. Excellent sets of these curvefits may be found in References [8], [9], and [10].

Since enthalpy is an extensive property, the enthalpy of the mixture is simply the sum of the enthalpies of the individual species:

$$h = \sum_{j=1}^{n_s} h_j^0 \sigma_j \tag{2.10}$$

where h_j^0 is the enthalpy of the j th species.

In addition, the molecular weight of the mixture is

$$w = \frac{1}{\sum_{j=1}^{n_s} \sigma_j} \tag{2.11}$$

The method for determining the values of the σ_j's will be discussed later for both finite rate and equilibrium flow.

Expressions are also assumed to be available for friction coefficient, work load, and heat losses (e.g. from boundary layer solutions). Although, as pointed out in the introduction, these terms will be considered negligible (C_f=dQ=dW=0), they will be retained for the sake of completeness throughout the algebraic development of the next few pages.

Equations (2.6) - (2.9) provide four equations for eight variables (dP, dρ, dw, dT, dV, dA, dh, and df). As mentioned above, the dh and dw terms may be found in terms of the other variables by using an appropriate gas model. The solution of the problem then only requires specifying two of the remaining six variables as independent functions of x.

In the development of the influence coefficient method, Shapiro introduces the relations for Mach number, M, and ratio of specific heats, γ, and then solves the above equations to provide a set of coefficients relating the dependent variables, $\frac{dM^2}{M^2}$, $\frac{dV}{V}$, $\frac{dT}{T}$, and $\frac{d\rho}{\rho}$ to such independent variables as $\frac{dA}{A}$, $\frac{d\dot{m}}{\dot{m}}$, $\frac{dw}{w}$,and $\frac{d\gamma}{\gamma}$. The coefficients derived are functions

of only the Mach number and the ratio of specific heats. Such a development is sufficient for perfect gases in which the Mach number and γ are well defined. However for a flow in which chemical reactions are occuring, both Mach number and γ lose meaning. Since the main focus of the work here is to study the effect of chemical reactions, M and γ are not introduced and the development of the equations is continued in terms of the primitive variables (P, T, V, h, etc).

2.3 Finite Rate Chemistry

This section develops the finite rate chemistry model following closely the development of Reference [11]. The fluid again is considered to be a gas mixture of n_s species with molar-mass concentrations σ_j . Between these chemical species, the chemical reactions are written in general as

$$\sum_{j=1}^{n_s} \nu_{ij}\, s_j = \sum_{j=1}^{n_s} \nu'_{ij} s_j \qquad i = 1, n_r \tag{2.12}$$

where s_j represent the chemical species, ν_{ij} represents the stoichiometric coefficient of the j^{th} species in the i^{th} reaction, and n_r is the number of reactions.

The forward production rate for a single reaction is

$$R_{f,i} = k_{f,i} \prod_{j=1}^{n_s} (\rho\, \sigma_j)^{\nu_{ij}} \qquad i = 1, n_r \tag{2.13}$$

where the forward rate constant, $k_{f,j}$, is given by the Arrhenius formula

$$k_{f,i} = A_i T^{n_i} \exp(-B_i/RT) \tag{2.14}$$

where A_i is the rate constant of reaction i, n_i is an exponent, and B_i is the activation energy for the reaction.

Likewise, the expression for the backward rate constant is

$$R_{b,i} = k_{b,i} \prod_{j=1}^{n_s} (\rho\, \sigma_j)^{\nu'_{ij}} \qquad i = 1, n_r \tag{2.15}$$

The forward and backward rate constants can also be related through

$$k_{b,i} = \frac{k_{f,i}}{K_{c,i}} \tag{2.16}$$

where $K_{c,i}$ is the equilibrium constant in concentration units.

The net production rate of species j is the difference between the forward and backward rates of production, namely

$$\frac{d\sigma_j}{dt} = \sum_{i=1}^{n_r} \frac{(\nu'_{ij} - \nu_{ij})}{\rho} k_{f,i} \left[\prod_{j=1}^{n_s} (\rho\,\sigma_j)^{\nu_{ij}} - \frac{1}{K_{c,i}} \prod_{j=1}^{n_s} (\rho\,\sigma_j)^{\nu'_{ij}} \right] + \frac{d\sigma_j^*}{dt} \tag{2.17}$$

where $\frac{d\sigma_j^*}{dt}$ represents an external source term of species j to account for mass addition to the flow.

Several of the reactions in the H_2-air reaction mechanism involve third bodies, M. In these reactions, any chemical species may act as the third body. The molar-mass fraction of the third body in reaction i is defined as

$$\sigma_{M,i} = \sum_{j=1}^{n_s} m_{i,j}\sigma_j \tag{2.18}$$

where $m_{i,j}$ is an 'efficiency factor' of the jth species in reaction i.

Equation (2.17) now provides a means of expressing the differential forms of Equations (2.10) and (2.11). For differentiation with respect to x:

$$\frac{dh}{dx} = \sum_{j=1}^{n_s} \sigma_j \frac{dh_j^0}{dT} \frac{dT}{dx} + \frac{1}{V} \sum_{j=1}^{n_s} h_j^0 \frac{d\sigma_j}{dt} \tag{2.19}$$

and

$$\frac{dw}{dx} = \frac{-1}{V(\sum_{j=1}^{n_s} \sigma_j)^2} \sum_{j=1}^{n_s} \frac{d\sigma_j}{dx} \tag{2.20}$$

Equations (2.19) and (2.20) can now be combined with Equations (2.6)-(2.11). Tables (2.1)-(2.3) present the solution of these flow equations in a manner analogous to the influence coefficients of Shapiro. Each table shows the dependence of the derivative in the left most column on the derivatives in the upper row, e.g.

$$\frac{dP}{P} = \frac{\mathcal{M}\mathcal{H}}{\mathcal{H}(1-\mathcal{M})-1} \frac{dA}{A} + \frac{\mathcal{M}(\mathcal{K}-2\mathcal{H}-1)}{\mathcal{H}(1-\mathcal{M})+1} \frac{df}{1+f} + \ldots \tag{2.21}$$

where

$$\mathcal{M} = \frac{\rho V^2}{P} \tag{2.22}$$

$$\mathcal{K} = \frac{h_T}{V^2} \tag{2.23}$$

$$\mathcal{H} = \sum_{j=1}^{n_s} \frac{\sigma_j C_{p,j}^0 T}{V^2} \tag{2.24}$$

$$C_{p,j}^0 = \frac{dh_j^0}{dT} \tag{2.25}$$

and

$$d\beta = dQ - dW \tag{2.26}$$

where dQ and dW are again the heat added to and work done by the fluid element, respectively.

The three tables show the coefficients for different independent variables. The independent variables in the tables are, respectively,

- Fuel fraction and Area
- Fuel fraction and Pressure
- Fuel fraction and Temperature

The solution of the flow equations requires simultaneously integrating the expressions shown in the tables with the species conservation equations of Equation (2.17).

2.4 Equilibrium Flow

An equilibrium flow solution is useful for comparison with the results of the finite rate case. This section develops the equations for equilibrium flow. The development is modelled after that of Reference [12]

If the gas mixture containing n_s species is ultimately comprised of n_e elements, each of the species may be expressed from a set of stoichiometric coefficients a_{ij} , such that a_{ij} gives the number of i atoms present in mole species j. The total number of atoms of each element per unit mass of the mixture, b_i^0 , can be found from the mass balance

$$b_i^0 = \sum_{j=1}^{n_s} a_{ij}\, \sigma_j \qquad\qquad i = 1, n_e \tag{2.27}$$

If the gas is in equilibrium, all thermodynamic properties of the gas are specified if two thermodynamic properties and the atomic composition (specified by knowing b_i^0) are known. Throughout this work, the most convenient thermodynamic variables are

Table 2.1: Influence Coefficients with Chemistry Added: Fuel and Area. The derivatives in the left most row are related to the derivatives in the upper column through the given coefficients.

	$\frac{dA}{A}$	$\frac{df}{1+f}$	$\frac{\sum_{j=1}^{n_s} h_i^0 \, d\sigma_j - d\beta}{\sum_{i=j}^{n_s} \sigma_j \, C_{p_j}^0 \, T}$	$\frac{dW}{W}$	$C_f \, \frac{dA_w}{2A}$
$\frac{dP}{P}$	$\frac{\mathcal{M}\mathcal{H}}{\mathcal{H}(1-\mathcal{M})-1}$	$\frac{\mathcal{M}(\mathcal{K}-2\mathcal{H}-1)}{\mathcal{H}(1-\mathcal{M})+1}$	$\frac{-\mathcal{H}\mathcal{M}}{\mathcal{H}(1-\mathcal{M})+1}$	$\frac{\mathcal{M}\mathcal{H}}{\mathcal{H}(1-\mathcal{M})+1}$	$\frac{-\mathcal{M}(\mathcal{H}+1)}{\mathcal{H}(1-\mathcal{M})+1}$
$\frac{dT}{T}$	$\frac{1}{\mathcal{H}(1-\mathcal{M})+1}$	$\frac{(1-\mathcal{M})(1-\mathcal{K})-2}{\mathcal{H}(1-\mathcal{M})+1}$	$-\frac{(1-\mathcal{M})\mathcal{H}}{\mathcal{H}(1-\mathcal{M})+1}$	$\frac{1}{\mathcal{H}(1-\mathcal{M})+1}$	$\frac{-\mathcal{M}}{\mathcal{H}(1-\mathcal{M})+1}$
$\frac{dV}{V}$	$\frac{-\mathcal{H}}{\mathcal{H}(1-\mathcal{M})+1}$	$\frac{\mathcal{H}(\mathcal{M}+1)-\mathcal{K}}{\mathcal{H}(1-\mathcal{M})+1}$	$\frac{-\mathcal{H}}{\mathcal{H}(1-\mathcal{M})+1}$	$\frac{-\mathcal{H}}{\mathcal{H}(1-\mathcal{M})+1}$	$\frac{\mathcal{H}\mathcal{M}}{\mathcal{H}(1-\mathcal{M})+1}$

Table 2.2: Influence Coefficients with Chemistry Added: Fuel and Pressure.The derivatives in the left most row are related to the derivatives in the upper column through the given coefficients.

	$\frac{dP}{P}$	$\frac{df}{1+f}$	$\frac{\sum_{j=1}^{n_s} h_j^0 \, d\sigma_j - d\beta}{\sum_{j=1}^{n_s} \sigma_j \, C_{p_j}^0 \, T}$	$\frac{dW}{W}$	$C_f \, \frac{dA_w}{2A}$
$\frac{dA}{A}$	$\frac{\mathcal{H}(1-\mathcal{M})+1}{\mathcal{M}\mathcal{H}}$	$\frac{2\mathcal{H}+1-\mathcal{K}}{\mathcal{H}}$	-1	-1	$\frac{\mathcal{H}+1}{\mathcal{H}}$
$\frac{dT}{T}$	$\frac{1}{\mathcal{H}\mathcal{M}}$	$\frac{1-\mathcal{K}}{\mathcal{H}}$	-1	0	$\frac{1}{\mathcal{H}}$
$\frac{dV}{V}$	$-\frac{1}{\mathcal{M}}$	-1	0	0	-1

Table 2.3: Influence Coefficients with Chemistry Added: Fuel and Temperature. The derivatives in the left most row are related to the derivatives in the upper column through the given coefficients.

	$\frac{dT}{T}$	$\frac{df}{1+f}$	$\frac{\sum_{j=1}^{n_s} h_j^0 \, d\sigma_j - d\beta}{\sum_{j=1}^{n_s} \sigma_j \, C_{p_j}^0 \, T}$	$\frac{dW}{W}$	$C_f \, \frac{dA_w}{2A}$
$\frac{dP}{P}$	$\mathcal{H}\mathcal{M}$	$\mathcal{M}(\mathcal{K}-1)$	$-\mathcal{H}\mathcal{M}$	0	$-\mathcal{M}$
$\frac{dA}{A}$	$1+\mathcal{H}(1-\mathcal{M})$	$1+\mathcal{M}+\mathcal{K}(1-\mathcal{M})$	$\mathcal{H}(1-\mathcal{M})$	-1	$\mathcal{M}$
$\frac{dV}{V}$	$-\mathcal{H}$	$-\mathcal{K}$	$\mathcal{H}$	0	0

pressure and temperature. With this functional dependence of h=h(P,T,b_i) in mind, the differentiation of Equations (2.10) and (2.11) yields

$$dh = (\frac{\partial h}{\partial T})\,dT + (\frac{\partial h}{\partial P})\,dP + \sum_{i=1}^{n_e}(\frac{\partial h}{\partial b_i^0})\,db_i \tag{2.28}$$

and

$$dw = (\frac{\partial w}{\partial T})\,dT + (\frac{\partial w}{\partial P})\,dP + \sum_{i=1}^{n_e}(\frac{\partial w}{\partial b_i})\,db_i \tag{2.29}$$

Expanding Equations (2.10) and (2.11) and substituting into Equations (2.28) and (2.29),

$$\begin{aligned} dh \;=\; & (\sum_{j=1}^{n_s}\frac{\partial h_j^0}{\partial T}\sigma_j + \sum_{j=1}^{n_s} h_j^0\frac{\partial \sigma_j}{\partial T})\,dT + (\sum_{j=1}^{n_s} h_j^0\frac{\partial \sigma_j}{\partial P})\,dP \\ & + \sum_{i=1}^{n_e}(\sum_{j=1}^{n_s} h_j^0\frac{\partial \sigma_j}{\partial b_i^0})\,db_i \end{aligned} \tag{2.30}$$

and

$$dw = \frac{-1}{(\sum_{j=1}^{n_s}\sigma_j)^2}\left[(\sum_{j=1}^{n_s}\frac{\partial \sigma_j}{\partial T})\,dT + (\sum_{j=1}^{n_s}\frac{\partial \sigma_j}{\partial P})\,dP + \sum_{i=1}^{n_e}(\sum_{j=1}^{n_s}\frac{\partial \sigma_j}{\partial b_i})\,db_i\right] \tag{2.31}$$

where the equilibrium values of σ_j and the partial derivatives have yet to be found as functions of P, T and b_i^0.

First, to find the values of σ_j , the requirements for a gas to be in equilibrium are considered. Since the specified variables are pressure and temperature, the proper requirement for equilibrium is the minimization of the Gibb's free energy. For the mixture of gases, the free energy is [5]

$$g = \sum_{j=1}^{n_s}\mu_j\,\sigma_j \tag{2.32}$$

where μ_j is the chemical potential defined as

$$\mu_j = (\frac{\partial g}{\partial \sigma_j})_{T,P,\sigma_{i\neq j}} \tag{2.33}$$

Equilibrium requires the minimization of Equation (2.32) subject to the mass constraint of Equation (2.27). Introducing the Lagrange multipliers, λ_i, gives the following:

$$G \equiv g + \sum_{i=1}^{n_e}\lambda_i(\sum_{j=1}^{n_s} a_{ij}\sigma_j - b_i^0) = 0 \tag{2.34}$$

Differentiation gives

$$\delta G = \sum_{j=1}^{n_s} \mu_j \delta n_j + \sum_{i=1}^{n_e} \delta\lambda_i \left(\sum_{j=1}^{n_s} a_{ij}\, \sigma_j - b_i^0\right) + \sum_{i=1}^{n_e} \left(\lambda_i \sum_{j=1}^{n_s} a_{ij}\, \delta\sigma_j\right) = 0 \tag{2.35}$$

Or, rearranging,

$$\sum_{j=1}^{n_s} \left(\mu_j + \sum_{i=1}^{n_e} \lambda_i a_{ij}\right) \delta\sigma_j + \sum_{i=1}^{n_e} \left(\sum_{j=1}^{n_s} a_{ij}\, \sigma_j - b_i^0\right) \delta\lambda_i = 0 \tag{2.36}$$

Each of the bracketed terms in Equation (2.36) must independently be zero. The second term again yields the mass constraint. The first term, however, introduces the further requirement that

$$\mu_j + \sum_{i=1}^{n_e} \lambda_i\, a_{ij} = 0 \tag{2.37}$$

For a thermally perfect gas, the chemical potential is given by

$$\mu_j = \mu_j^0 + RT \ln \frac{\sigma_j}{\sigma_{tot}} + RT \ln P \qquad\qquad j = 1, n_s \tag{2.38}$$

where μ_j^0 is the chemical potential of the j^{th} species in the standard state, R is the universal gas constant, and σ_{tot} is the total number of moles per unit mass of mixture,

$$\sigma_{tot} = \sum_{j=1}^{n_s} \sigma_j \tag{2.39}$$

Combining Equations (2.27), (2.37), (2.38), and (2.39) now provides a set of nonlinear algebraic equations, the solution of which provides the equilibrium composition of the gas mixture:

$$\begin{cases} b_i^0 = \sum_{j=1}^{n_s} a_{ij}\, \sigma_j & i = 1, n_e \\ \mu_j^0 + RT \ln \frac{\sigma_j}{\sum_{j=1}^{n_s} \sigma_j} + RT \ln P + \sum_{i=1}^{n_e} \lambda_i\, a_{ij} = 0 & j = 1, n_s \end{cases} \tag{2.40}$$

Equation (2.40) provides $n_e + n_s$ equations for the $n_e + n_s$ unknowns ($n_e\ \lambda's\ and\ n_s\ \sigma's$). The non-linear set of equations in general requires an iterative solution such as the Newton-Raphson method.

With the equilibrium values of the σ_j 's determined from the solution of the nonlinear set of equations, the partial derivatives of the enthalpy and molecular weight may be

found. Equations (2.30) and (2.31) ultimately require the partial derivatives with respect to pressure, temperature, and atomic composition (b_i^0). For the sake of brevity, let the parameter z be any one of these quantities.

Differentiation of Equations (2.27), (2.38) and (2.39) yields

$$\sum_{j=1}^{n_s} a_{ij} \frac{\partial \sigma_j}{\partial z} - \frac{\partial b_i^0}{\partial z} = 0 \qquad i = 1, \ell \tag{2.41}$$

$$\frac{1}{\sigma_j} \frac{\partial \sigma_j}{\partial z} - \frac{1}{\sigma_{tot}} \frac{\partial \sigma_{tot}}{\partial z} + \frac{1}{P} \frac{\partial P}{\partial z} + \sum_{i=1}^{\ell} \frac{\partial \pi_i}{\partial z} a_{ij} = 0 \qquad j = 1, n_s \tag{2.42}$$

where $\pi_i = -\frac{\lambda}{RT}$, and

$$\frac{\partial \sigma_{tot}}{\partial z} = \sum_{j=1}^{n_s} \frac{\partial \sigma_j}{\partial z} \tag{2.43}$$

Equations (2.41), (2.42), and (2.43) provide $m+\ell+1$ equations for $m+\ell+1$ unknowns (ℓ $\frac{\partial \pi_i}{\partial z}$, m $\frac{\partial \sigma_j}{\partial z}$, and $\frac{\partial \sigma_{tot}}{\partial z}$). Unlike the equations for the σ_j's however, these equations are linear and can easily be solved once the equilibrium concentrations are known.

Knowing the expressions for the equilibrium composition of the gas and the partial derivatives, Equations (2.6)-(2.11), (2.30) and (2.31) may be combined to provide a set of four equations for six unknowns. Since the interest here is the flow in a combustor and nozzle, the variables of interest are V, P, T, and f. As in the finite rate solution, the equations may be solved for different sets of independent variables. The solution is provided below for the following combinations of independent variables:

- Temperature and area
- Pressure and area
- Fuel fraction and area
- Temperature and fuel fraction
- Pressure and fuel fraction

To reduce the rather extensive algebra, the following nondimensional variables are defined:

$$\begin{aligned} \mathcal{M} &= \frac{\rho V^2}{P} \\ \mathcal{K} &= \frac{h_T}{V^2} \end{aligned} \tag{2.44}$$

$$
\begin{aligned}
\omega_H &= \frac{1}{w}\left(\frac{\partial w}{\partial b_i^0}\right)(1+f) \\
\omega_P &= \frac{1}{w}\left(\frac{\partial w}{\partial P}\right)P \\
\omega_T &= \frac{1}{w}\left(\frac{\partial w}{\partial T}\right)T \\
S_H &= \frac{1}{V^2}\left(\frac{\partial h}{\partial b_i^0}\right)(1+f) \\
S_P &= \frac{1}{V^2}\left(\frac{\partial h}{\partial P}\right)P \\
S_T &= \frac{1}{V^2}\left(\frac{\partial h}{\partial T}\right)T
\end{aligned}
\tag{2.45, 2.46}
$$

as well as the following convenient groupings:

$$
\begin{aligned}
a &= \omega_H - 1 \\
b &= 1 + \omega_P - \frac{1}{\mathcal{M}} \\
c &= S_H - 1 + \frac{\mathcal{K}}{V^2} \\
d &= \omega_H - 2 \\
e &= S_P - \frac{1}{\mathcal{M}}
\end{aligned}
\tag{2.47}
$$

$$
\begin{aligned}
\frac{dV^*}{V^*} &= -\left\{\frac{1}{\mathcal{M}}\frac{dP}{P} + \frac{df}{1+f} + \frac{C_f}{2A}dA_w\right\} \\
\frac{dT^*}{T^*} &= -\frac{b}{a}\frac{dP}{P} - \frac{d}{a}\frac{df}{1+f} - \frac{1}{a}\frac{C_f}{2A}dA_w - \frac{1}{a}\frac{dA}{A} \\
\frac{dP^*}{P^*} &= -\frac{a}{b}\frac{dT}{T} - \frac{d}{b}\frac{df}{1+f} + \frac{1}{b}\frac{C_f}{2A}dA_w - \frac{1}{b}\frac{dA}{A} \\
\frac{df^*}{1+f^*} &= \frac{a\,e - b\,S_T}{d\,S_T\,d - a\,c}\frac{dP}{P} - \frac{a}{S_T\,d - a\,c}\frac{d\beta}{V^2} - \frac{a - S_T}{S\,d - a\,c}\frac{C_f}{2A}dA_w - \\
&\qquad \frac{S_T}{S_T\,d - a\,c}\frac{dA}{A}
\end{aligned}
\tag{2.48}
$$

With these definitions, the equations may be written as a series of coefficients similar to those given in the finite rate solution. The algebraic complexity, however, prevents this. Instead, after making the above substitutions, the flow equations are written:

- Temperature and area

$$\begin{cases} \dfrac{df}{1+f} = \dfrac{a\,c - d\,S_T}{d\,c - b\,c}\dfrac{dT}{T} - \dfrac{b}{d\,e - b\,c}\dfrac{d\beta}{V^2} - \dfrac{b - e}{d\,e - b\,c}\dfrac{C_f}{2\,A}dA_w - \dfrac{e}{d\,e - b\,c}\dfrac{dA}{A} \\ \dfrac{dP}{P} = \dfrac{dP^*}{P^*} \\ \dfrac{dV}{V} = \dfrac{dV^*}{V^*} \end{cases} \tag{2.49}$$

- Pressure and Area

$$\begin{cases} \dfrac{df}{1+f} = \dfrac{a\,e - b}{S_t\,d - a\,c}\dfrac{dP}{P} - \dfrac{a}{d\,S_T - a\,c}\dfrac{d\beta}{V^2} - \dfrac{a - S_T}{S_T\,d - a\,c}\dfrac{C_f}{2\,A}dA_w - \dfrac{S_T}{S_T\,d - a\,c}\dfrac{dA}{A} \\ \dfrac{dT}{T} = \dfrac{dT^*}{T^*} \\ \dfrac{dV}{V} = \dfrac{dV^*}{V^*} \end{cases} \tag{2.50}$$

- Fuel fraction and Area

$$\begin{cases} \dfrac{dP}{P} = -\dfrac{a\,c - d\,S_T}{a\,e - b}\dfrac{df}{1+f} + \dfrac{a}{a\,e - b}\dfrac{d\beta}{V^2} + \dfrac{a - 1}{a\,e - b}\dfrac{C_f}{2\,A}dA_w + \dfrac{S_T}{a\,e - b}\dfrac{dA}{A} \\ \dfrac{dT}{T} = \dfrac{dT^*}{T^*} \\ \dfrac{dV}{V} = \dfrac{dV^*}{V^*} \end{cases} \tag{2.51}$$

- Temperature and fuel fraction

$$\begin{cases} \dfrac{dA}{A} = \dfrac{a\,c - d\,S_T}{e}\dfrac{dT}{T} - \dfrac{d\,e - b\,c}{e}\dfrac{df}{1+f} - \dfrac{b - e}{e}\dfrac{C_f}{2\,A}dA_w - \dfrac{b}{e}\dfrac{d\beta}{V^2} \\ \dfrac{dP}{P} = \dfrac{dP^*}{P^*} \\ \dfrac{dV}{V} = \dfrac{dV^*}{V^*} \end{cases} \tag{2.52}$$

- Pressure and fuel fraction

$$\begin{cases} \dfrac{dA}{A} = \dfrac{a\,e-b}{S_T}\dfrac{dP}{P} - \dfrac{a}{S_T}\dfrac{d\beta}{V^2} - \\ \qquad \dfrac{a-S_T}{S_T}\dfrac{C_f}{2\,A}dA_w - \dfrac{d\,S_T - a\,c}{S_T}\dfrac{df}{1+f} \\ \dfrac{dT}{T} = \dfrac{dT^*}{T^*} \\ \dfrac{dV}{V} = \dfrac{dV^*}{V^*} \end{cases} \tag{2.53}$$

The flow solution requires simultaneously integrating the equations above for the desired independent variables. The values of the chemical composition must be found at each point in the integration through the solution of the nonlinear algebraic equations given in Equation (2.40).

2.5 Numerical Solution

Finite Rate

Although algebraically much simpler than the equilibrium solution, the finite rate equations are much more difficult to numerically integrate. The vastly varying time scales of the reactions cause the equations to be quite stiff. Such standard integration methods as Runge-Kutta require unacceptably small integration steps to maintain stability. Instead, the equations are integrated using the variable order, variable step, stiffly stable predictor-corrector method of C.W. Gear (see References [13] and [14]). The methodology of the integration procedure is as follows: Given the information on a datum, the net production rates of the species can be calculated from Equation (2.17). All information is then known to solve for the derivatives of the flow variables given in Tables (2.1)-(2.3). The flow properties are then stepped forward to obtain the information at the new datum.

Equilibrium

A numerical solution to the equilibrium equations can be obtained from any standard integration technique. The method used for this thesis was a fourth order Runge-Kutta integration. The methodology is as follows: Assume the flow properties (P, T, V and f) and atomic compositions are known along a given datum. From the atomic composition, pressure and temperature, Equation (2.40) can be solved to provide the equilibrium molar-mass fractions, σ_j. (The solution of the large set of simultaneous nonlinear equations

is not in general easy, especially in the present case when the solution vector of σ_j's may contain elements varying by as much as thirty orders of magnitude. An efficient algorithm for the solution of these equations is discussed by D.R. Cruise [15]. The method first chooses a subset of molecular species from which all the other species may be formed by chemical reaction. Then, using the Gibb's free energy, the discrepancy in the equilibrium relations are computed. Finally, the species farthest from equilibrium are corrected stoichiometrically until convergence is obtained. The reader is referred to Cruise's paper for further information). Knowing the equilibrium species concentrations, the necessary partial derivatives may be calculated by solving the resulting set of linear equations (2.41), (2.42), and (2.43). This then provides all the necessary information to step forward the appropriate set of equations for the specified independent variables. All new information is then known on the new datum and the integration may proceed.

Chapter 3

Inlet Results

This chapter presents the results of the inlet model. As mentioned in the derivation of the inlet model, the solution of the global conservation equations for the inlet control volume requires specifying a design point. This study will consider two design points. The first design point provides approximately 1200 K at the combustor entrance at a flight Mach number of 10. This design point is chosen to provide minimum temperatures at the combustor inlet of approximately 800 K at a Mach number of 5. The required ramp angles for this case are 8.31 degrees. A second design point will also be considered. This design point is chosen to limit the temperature at the upper end of the trajectory to 2400 K. At 30 km and M=10, this inlet delivers flow to the combustor at 718 K. The ramp angles are 5.07 degrees.

Figure 3.1 shows the pressure and temperature at the combustor entrance as a function of flight Mach Number and altitude for the first design point. The solid, approximately horizontal lines represent isobars at the combustor entrance ranging from 0.01 to 5.0 atm. The dotted, vertical lines are isotherms. This trajectory shows that, in order to maintain 800 K at M=5, temperatures of approximately 3400 K must be accepted at M=25. To maintain 0.05 atm at the combustor entrance, the altitude must range from about 45 km at Mach 5 to 60 km at Mach 17.5. Likewise, 5.0 atm is maintained for flight at approximately 15 km at Mach 5 and 25 km at Mach 25.

Also of concern in the kinetic studies is the residence time of a fluid element in the combustor. Figure 3.2 plots the inverse of the velocity as a function of Mach number and altitude. The result is a plot of the time required for a fluid particle to traverse one meter, assuming constant velocity. For a combustor on the order of 1.0 m in length, the residence times range from about 0.8 ms at Mach 5 to less than 0.2 ms at Mach 25.

Figure 3.3 shows the pressure and temperature of the fluid delivered to the beginning of the combustor for the second design point. Although the temperatures at high Mach numbers are less than 2400 K, the temperatures at the low end of the trajectory now drop

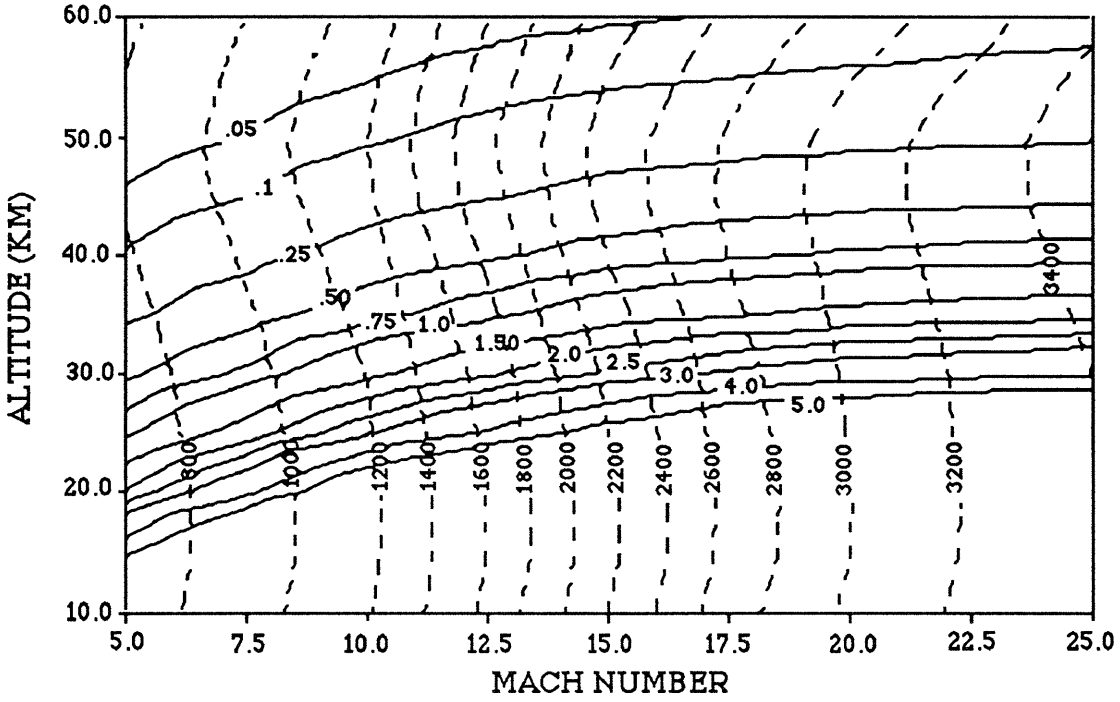

Figure 3.1: Pressure and temperature delivered to the combustor for the first design point. The dotted lines are isotherms marked in Kelvin. The solid lines are isobars marked in atmosphere.

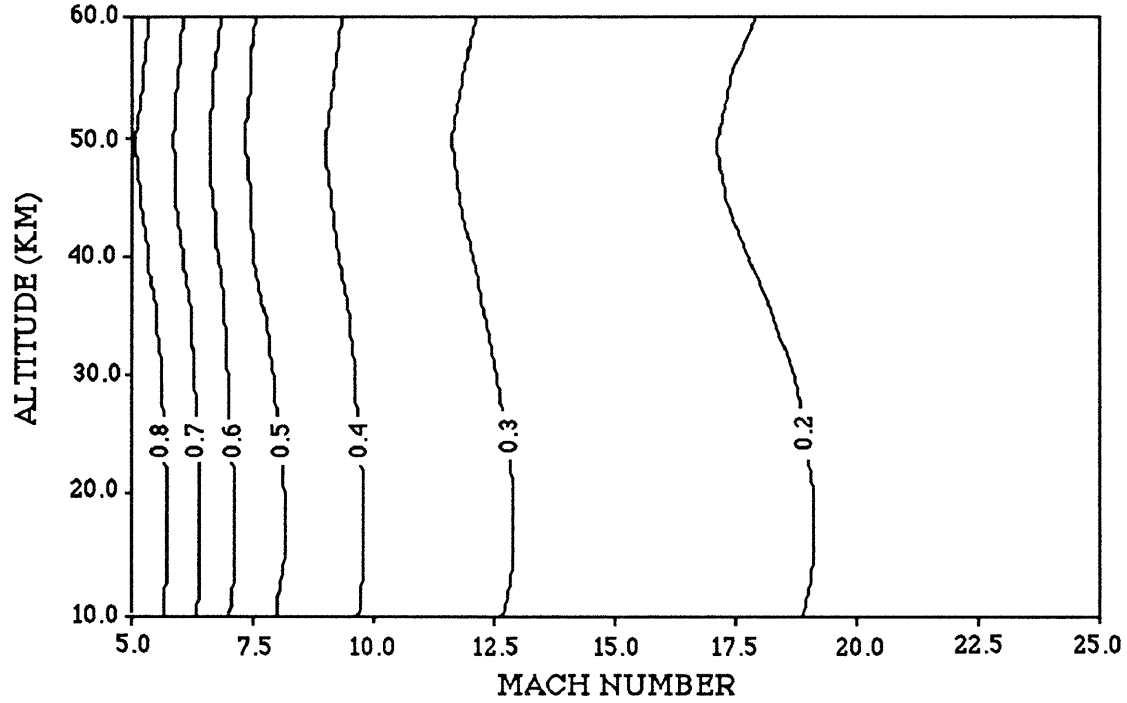

Figure 3.2: Residence time per meter of a fluid element in the combustor assuming constant velocity (first design point). The times marked are in milliseconds

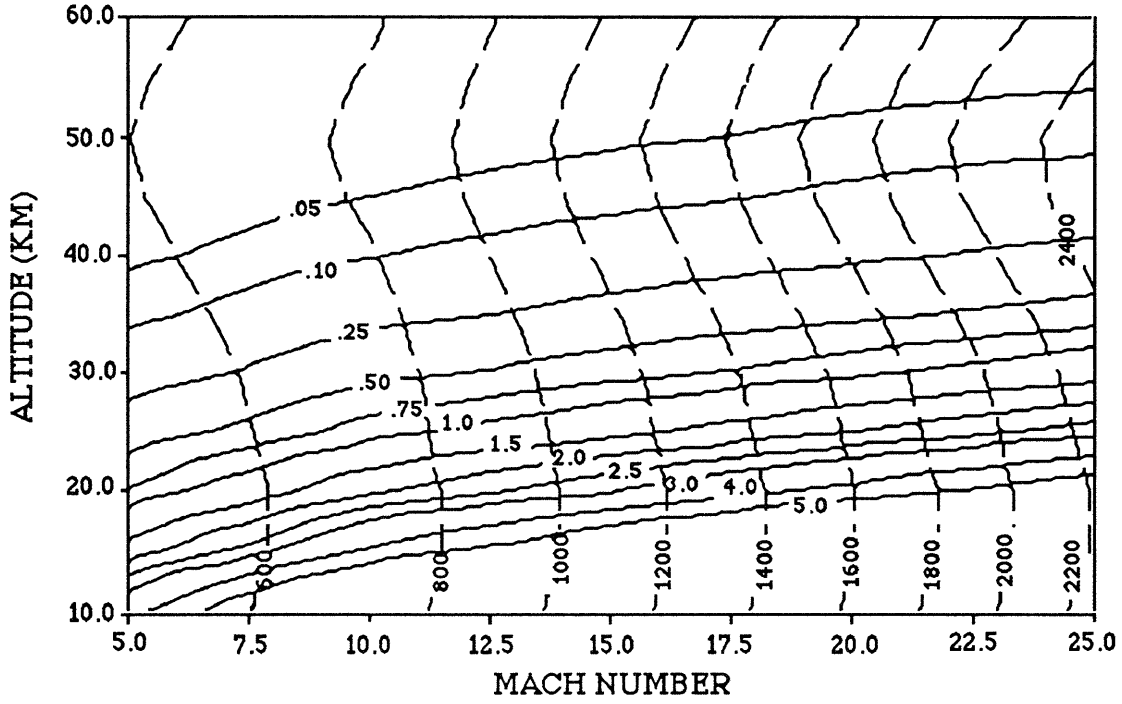

Figure 3.3: Pressure and temperature of the flow delivered to the combustor for the second design point. The dotted lines are isotherms marked in Kelvin. The solid lines are isobars marked in atmosphere.

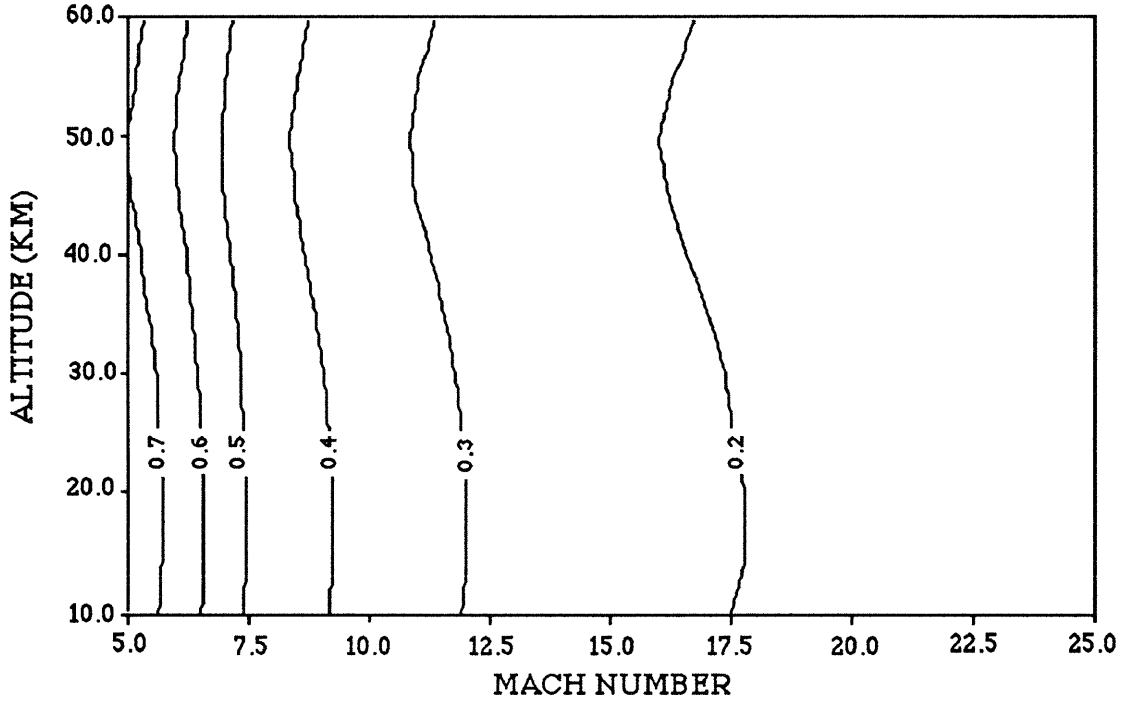

Figure 3.4: Residence time per meter in the combustor for the second design point. The lines are lines of constant residence time, marked in milliseconds.

to under 600 K. Also, because of the smaller ramp angle, the vehicle must fly a lower trajectory to maintain pressure in the combustor. Pressure at the combustor entrance is 0.5 atm for flight at Mach 5 at about 30 km and Mach 25 at 50 km. The pressure doesn't exceed 5.0 atm for flight above 10 km at Mach 6 or above 18 km at Mach 25. Figure 3.4 shows the residence time per meter of combustor. The residence times per meter are seen to range from slightly above 0.7 ms at Mach 5 to less than 0.2 ms at Mach 25.

Chapter 4

Static Reaction Results

A simple model that provides insight into the underlying nature of the combustion process in the SCRAMJET engine is to consider the SCRAMJET as the combustion chamber in a simple Brayton cycle. The combustion process must, then, by definition, occur at constant pressure. If the details of the injection process are ignored, the momentum equation assures that the velocity is also constant. In this model, the reactions occurring in the SCRAMJET are the same as would occur in a static, constant pressure reaction. The static, constant pressure model is in fact quite useful for investigating the ignition limits and reaction times of a combusting gas. The following sections discuss static, constant pressure reactions for three gas mixtures. The first section examines the H_2-air reaction that forms the basis for the SCRAMJET combustion process. As discussed below, however, the combustion limits and reaction times of H_2-air combustion make ignition aids necessary over some portions of the trajectory. Two fuel additives are discussed: hydrogen peroxide and silane.

4.0.1 Hydrogen-Air System

The first case considered is hydrogen (H_2) combustion in air, where air at standard sea level conditions is

- 78% Diatomic Nitrogen
- 21% Diatomic Oxygen
- 1% Argon

The reaction mechanism is based on that of Rogers and Schexnayder [11] and consists of 12 species (H_2 ,O_2 ,N_2 ,H ,O ,N ,Ar ,H_2O ,OH ,HO_2 ,H_2O_2 , and NO) and 23 reaction paths. Table A.3 (see Appendix A) contains the reactions and the values of the constants for the Arrenhius rate expression in the form of Equation (2.14). Also in Appendix A are the curve fits used for enthalpy calculations.

Using the data shown in the appendix, the kinetic equations of Table 2.2 can be integrated forward in time. Figures 4.1 and 4.2 represent a typical reaction history. The reaction has two distinct phases. The first section of the reaction (0 <T<.25 mS) is the exponential growth of the free radicals caused by the bimolecular dissociation of H_2 and O_2 (Figure 4.1). During this section of the reaction, the temperature also undergoes an exponential increase (Figure 4.2). In the second part of the reaction, the species begin relaxing to their equilibrium values through a series of relatively slow third body reactions. The temperature still increases substantially in this part of the reaction since much of the reaction's energy is released during the recombination of free radicals.

Two methods for discussing the characteristic time of the reaction are in popular use. The ignition time is defined as the time from the beginning of the reaction to the peak value of OH, and the total reaction time is the time to reach 95% of the equilibrium temperature rise. Since the main concern in the combustor is the total heat release, the second definition will be used.

Figure 4.3 presents the total reaction time of the H_2-air system as a function of initial temperature and pressure for an equivalence ratio (the ratio of actual fuel to that required for stoichiometric reaction) of unity. The reaction times were calculated for an initial temperature range of 900 K-1400 K and a pressure range of 0.1-2.0 atm. These values are representative of the conditions expected inside a SCRAMJET combustor.

As clearly indicated in the figure, a strong nonlinearity in the 900 K and 1000 K curves occur at pressures of 0.3 and 1.0 atm respectively. This nonlinearity occurs as the H_2-air reaction nears its ignition limit.

The mechanism of the ignition limit can be understood by again referring to Figure 4.1. The rapid breakdown of H_2 and O_2 into free radicals is led by the creation of hydrogen peroxyl, HO_2. The major path of HO_2 formation is the third body reaction $M + H + O_2 = HO_2 + M$. Essentially, this chain breaking reaction depletes the supply of atomic hydrogen. Since the reaction is a third body reaction, the rate of reaction (and of atomic hydrogen depletion) increases with increased pressure. Since the formation of free radicals is vital in the initiation of the exponential portion of the reaction, the depletion of atomic hydrogen slows the entire reaction. If the rate of scavenging of H atoms exceeds the rate of H atom production, the reaction stops.

In order to provide regenerative cooling capabilities for the vehicles surface, the vehicle's SCRAMJET may actually be operated at an equivalence ratio in excess of 1.0. The reaction times for equivalence ratios greater than 1.0 are investigated in Figure 4.4. In general, increasing the equivalence ratio slightly increases the total reaction times. The

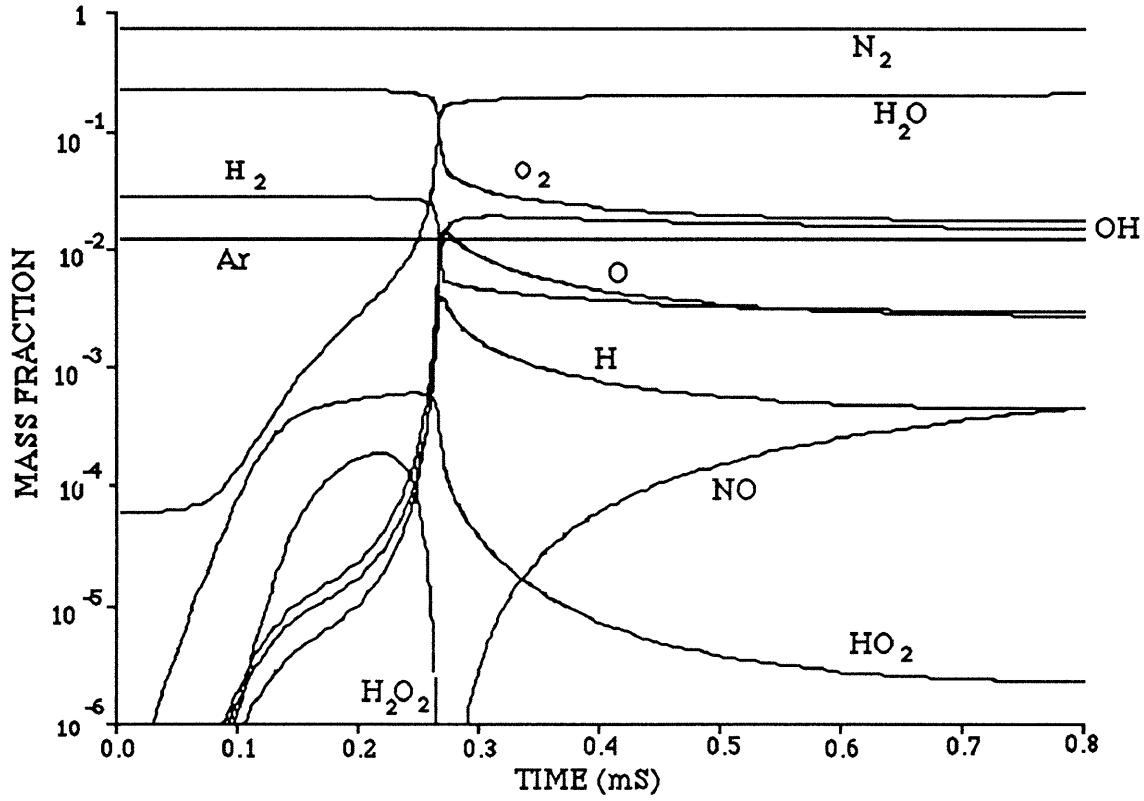

Figure 4.1: Time history of the mass fractions in a stoichiometric hydrogen-air reaction with an initial temperature of 1000 K and an initial pressure of 1 atm.

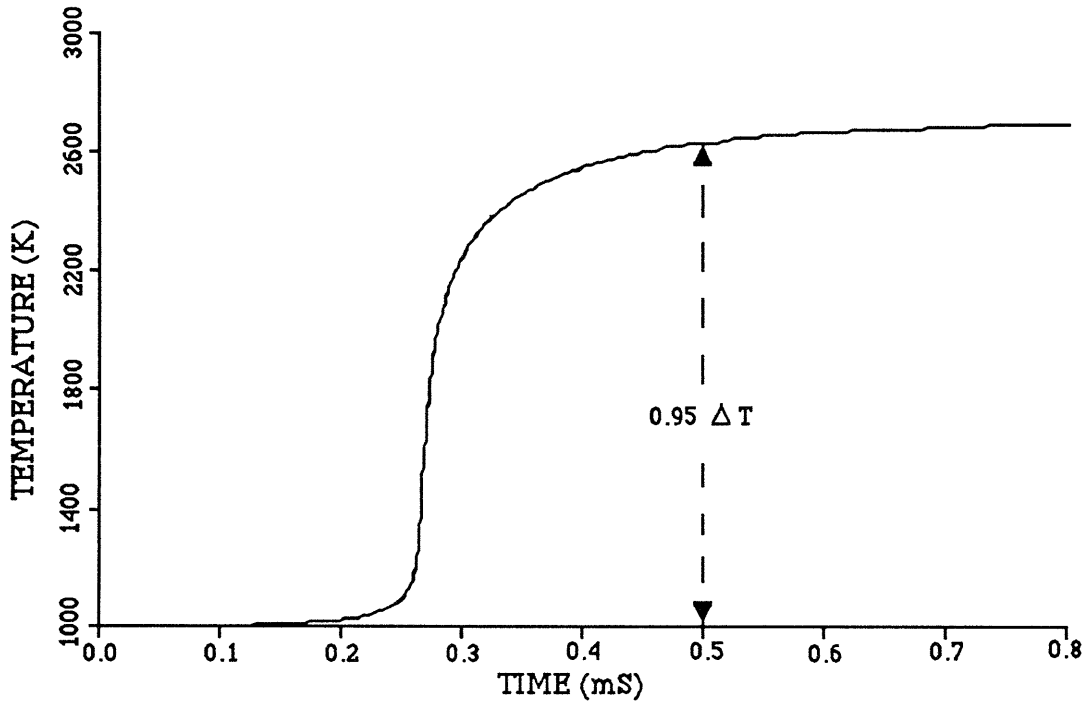

Figure 4.2: Time history of the temperature in a stoichiometric hydrogen-air reaction with an initial temperature of 1000 K and an initial pressure of 1 atm.

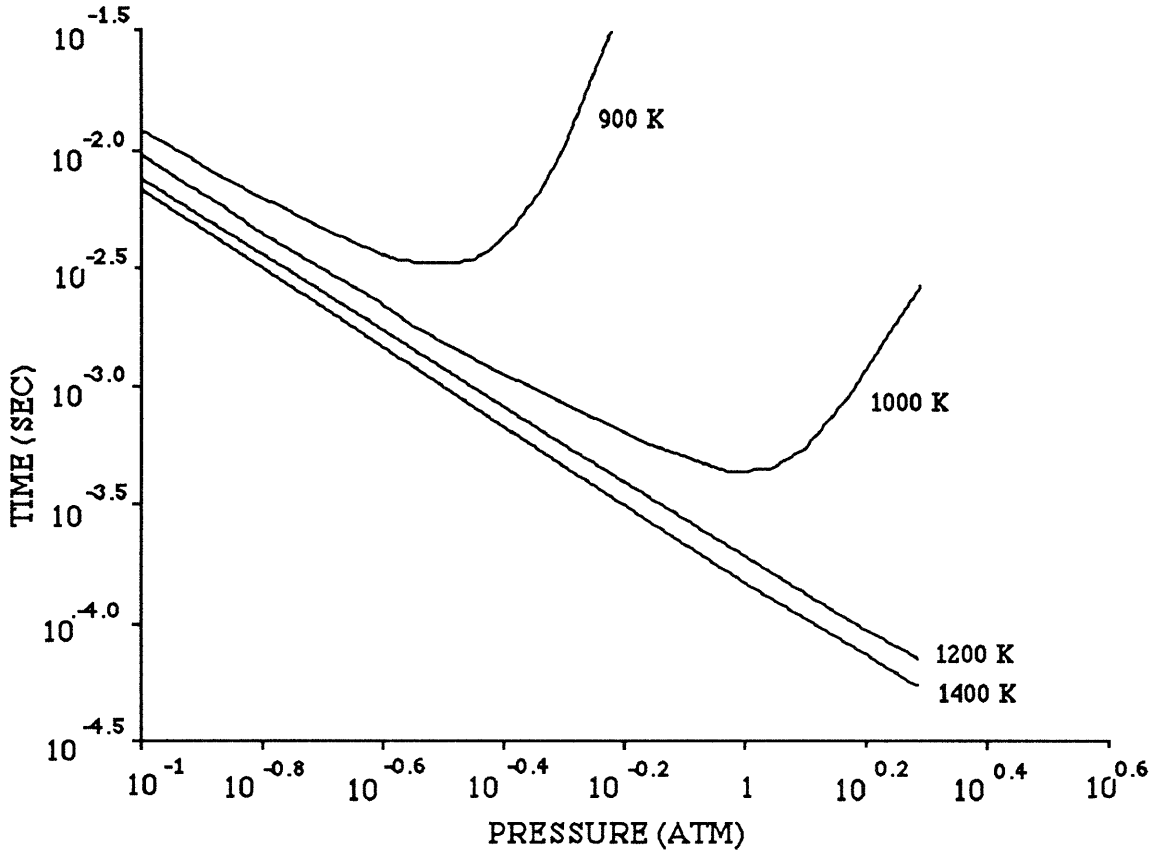

Figure 4.3: Total reaction times for the H_2-Air system as a function of initial temperature and pressure. The 900 K and 1000 K lines reach the ignition limit at 0.3 atm and 1.0 atm respectively.

effect is somewhat more noticeable above an equivalence ratio of about 2.5. The two dotted lines in the figure denote pressures above the minimum in the 900 K and 1000 K curves at an equivalence ratio of 1.0. These curves experience greater increased reaction times.

By combining the data of Figures (3.1), (3.2), and (4.3), the required combustor length for complete combustion can be found as a function of altitude and flight Mach number. Figures 4.5 and 4.6 show the required length of constant pressure combustor necessary for complete combustion at the first and second design points, respectively. The combustor lengths are plotted for pressures delivered to the combustor of between 0.1 and 2.0 atm. The low pressure limit is considered to be the limit of effective combustion. The high pressure limit is assumed to provide the lowest practical trajectory that satisfies other aerodynamic constraints on the vehicle. This lower trajectory limit is actually 10 to 20 km lower than the trajectories usually associated with hypersonic vehicles [16]. The lines in the figure are lines of constant combustor length, measured in meters. As clearly seen in

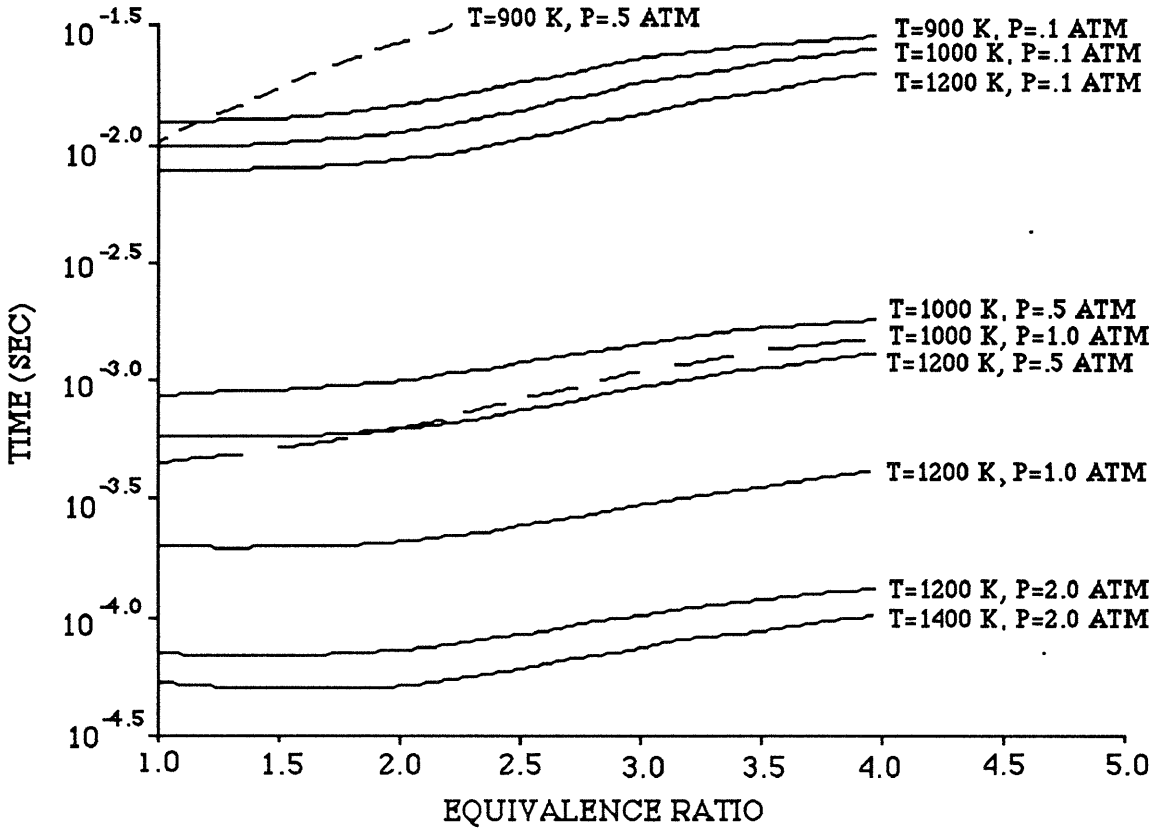

Figure 4.4: Effect of equivalence ratio on the H_2-Air reaction. The dotted lines denote curves for which the pressure is above that for minimum reaction time at an equivalence ratio of 1.0

the figures, the required combustor lengths become impractically long as the temperature nears the ignition limit of H_2. For the first design point, the ignition limit is reached for flight below approximately Mach 7.5. For the second design point, the ignition limit is reached below approximately Mach 12.5. Flight below these Mach numbers will required some type ignition aid to initiate combustion. The sections below discuss hydrogen peroxide and silane as possible ignition aids.

The necessity of maintaining sufficient pressure in the combustor can also be seen in Figures 4.5 and 4.6. At low pressures, the third body reactions are less effective, requiring longer combustor lengths to obtain full heat release. A comparison of Figures 4.5 and 4.6 with Figures 3.1 and 3.2 shows that the pressure delivered to the combustor must be greater than about 0.5 atm to maintain combustor lengths less the 3.0 m.

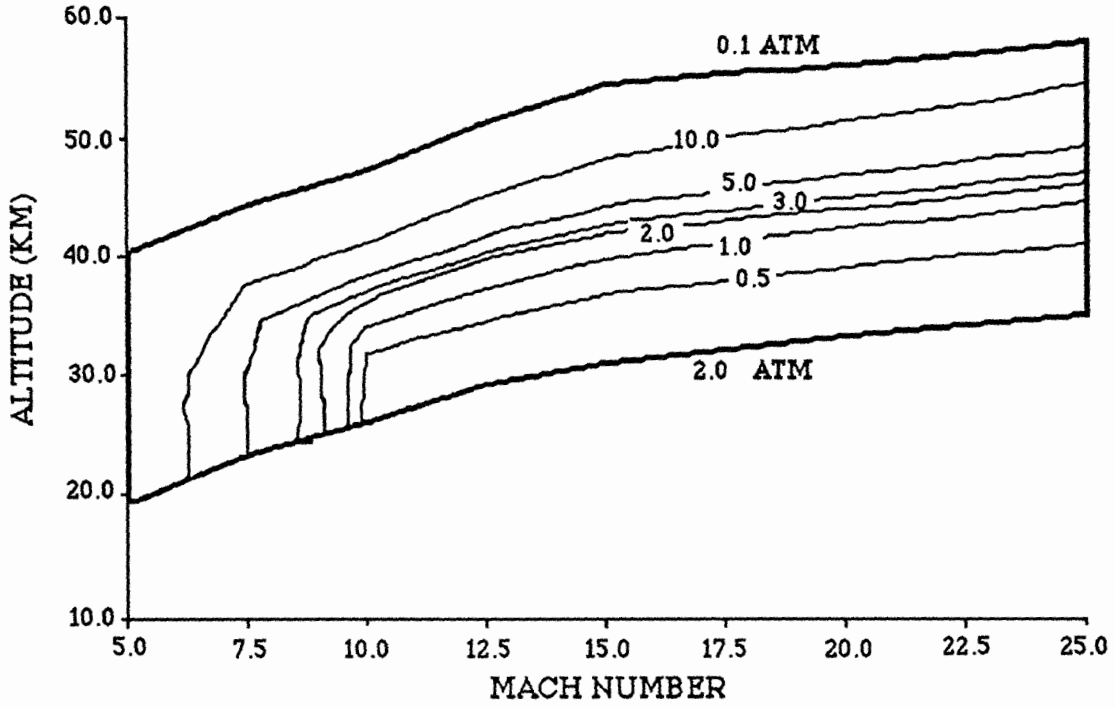

Figure 4.5: Required lengths of the combustor at the first design point for complete combustion to occur. The lines shown are lines of constant length in meters.

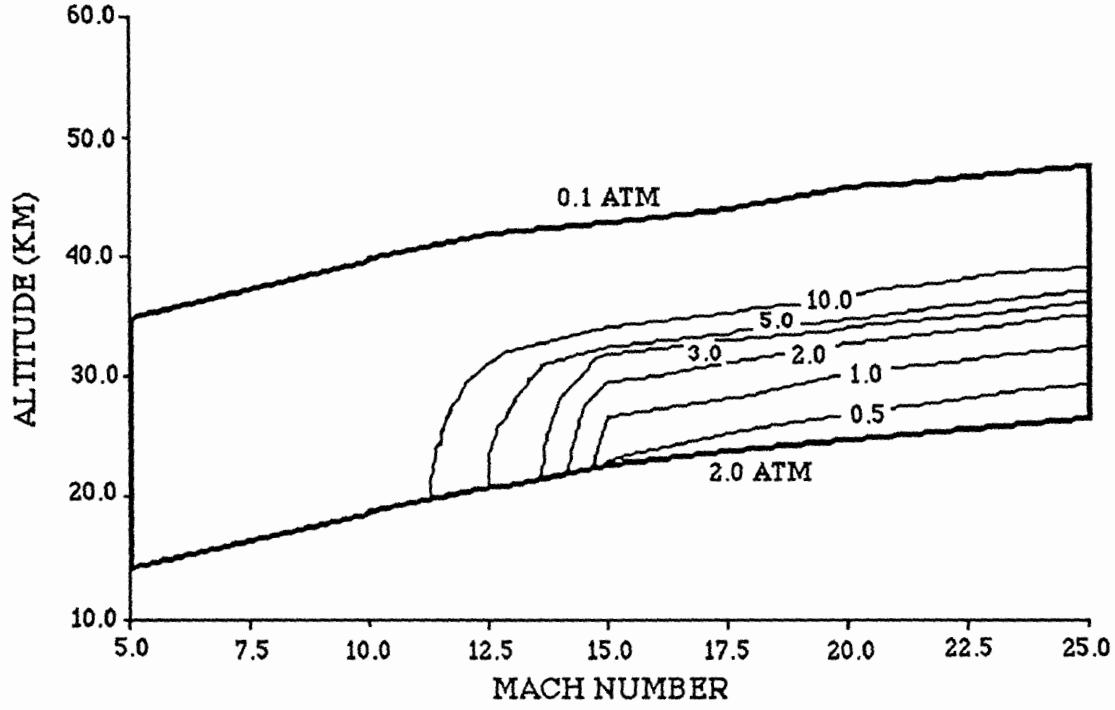

Figure 4.6: Required lengths of the combustor at the second design point for complete combustion to occur. The lines shown are lines of constant length in meters.

4.0.2 Hydrogen-Air-Hydrogen Peroxide System

As discussed above, an ignition aid will most likely be necessary over some portion of the trajectory. Hydrogen peroxide presents an easily available, inexpensive possibility of an ignition aid. The direct attack on the hydrogen peroxide molecule by both free radicals and diatomic molecules, as well as the third body decomposition, cause an abundant supply of free radicals to be produced in the initial stage of the hydrogen-air-hydrogen peroxide reaction. If the free radicals are produced by the decomposition of hydrogen peroxide faster than the scavenging by hydrogen peroxyl, the ignition limit will be overcome.

Figure 4.7 plots total reaction time versus initial temperature and pressure for a mixture of stoichiometric hydrogen/air and 2.5 % mass fraction hydrogen peroxide. The nonlinearity of the ignition limit is distinctly weakened in the 900 K and 1000 K lines. This is caused by the precise reason given above: the additional formation of free radicals by the decomposition of the hydrogen peroxide. The reaction times for initial temperatures greater than 1200 K are also slightly reduced.

The effect of increasing the mass fraction of H_2O_2 at other temperatures and pressures is investigated in Figure 4.8. At temperatures and pressures not affected by the ignition limit (solid lines), increasing amounts of H_2O_2 cause slight decreases in the total reaction times. For those temperatures and pressures that are effected by the ignition limit (dotted lines), however, the effect of hydrogen peroxide is to drastically reduce the total reaction times as the ignition limit is overcome.

The data presented so far has been for initial temperatures greater than 900 K. Unfortunately, hydrogen peroxide fails to provide an advantage at lower temperatures. Figure 4.9 shows the reaction time as a function of initial temperatures of 750-1000 K and mass fractions of 5% and 10% H_2O_2. Below 900 K, the reaction rates for the decomposition of H_2O_2 are severely reduced. The reduction in the rate of decomposition of H_2O_2 increases the total reaction time. To maintain total reaction times on the order of 1.0 ms, the initial temperature must be greater than about 850 K.

4.0.3 Hydrogen-Air-Silane System

Another possibility for an ignition aid is silane, SiH_4. Silane was used in the early ground testing of the Langley Hypersonic Research Engine to facilitate ignition in the subscale test engine.

Unlike H_2O_2, silane induces the hydrogen reaction to proceed through a thermal effect. Silane is highly reactive with air at room temperature. When mixed with a H_2-air system,

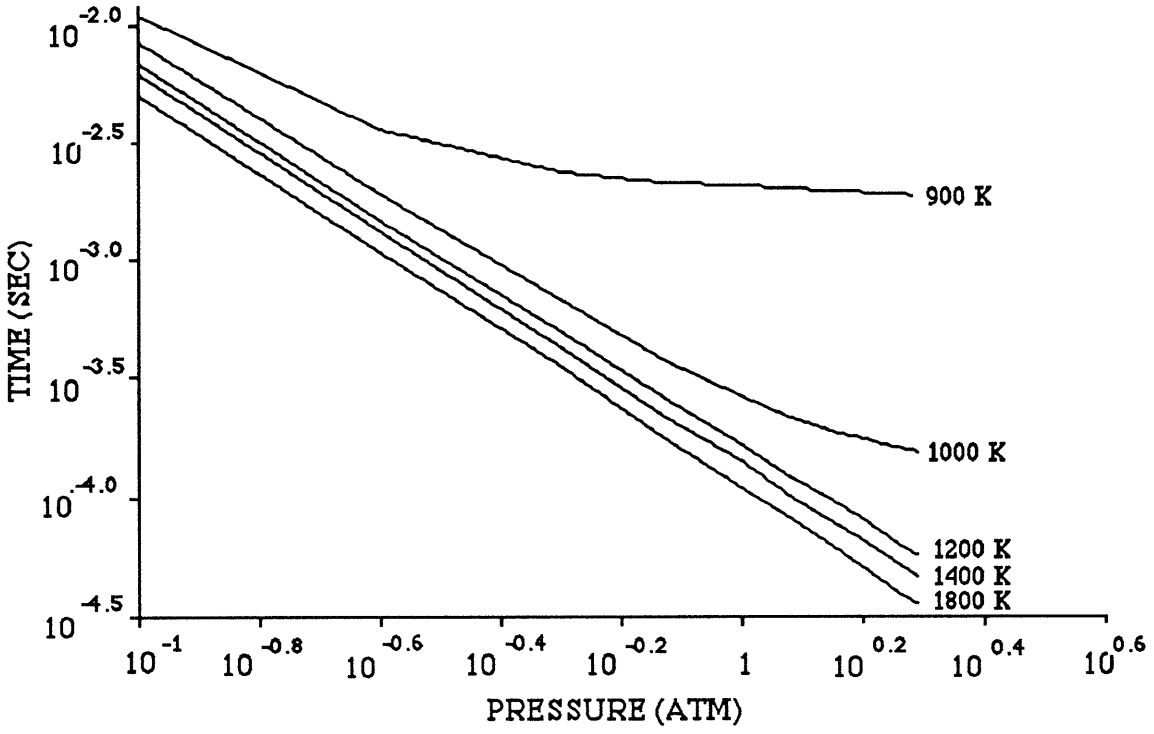

Figure 4.7: Total reaction times for the H2-air-2.5% H_2O_2 system as a function of initial temperature and pressure

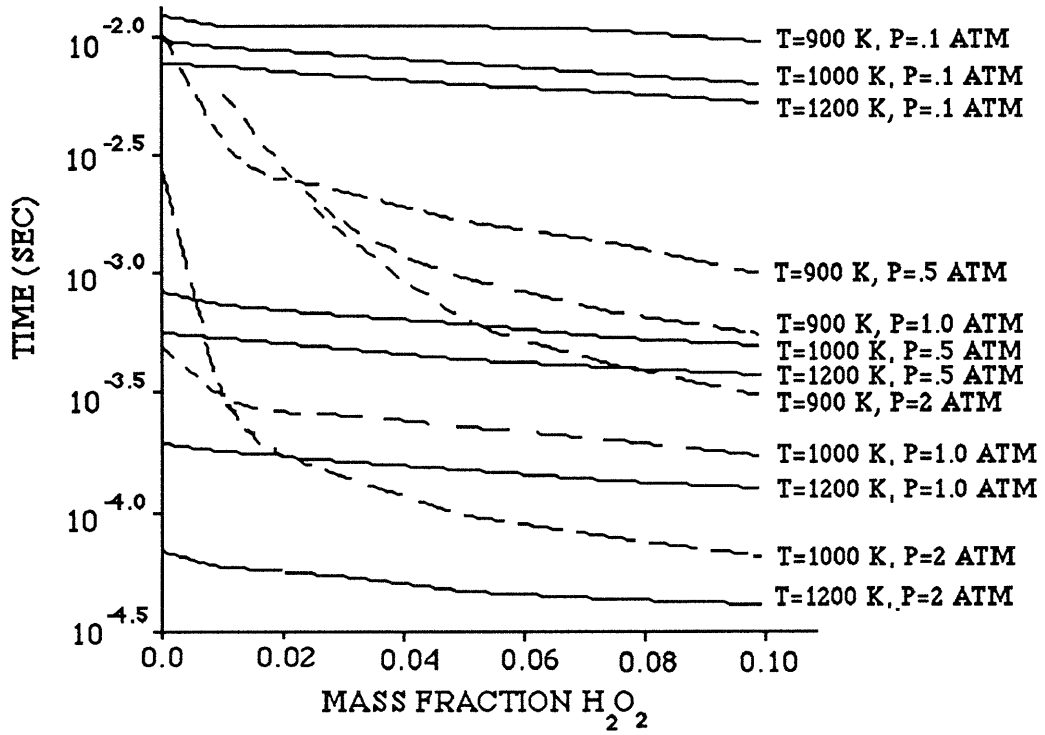

Figure 4.8: The effect of increased mass fraction of H_2O_2 on the total reaction time for various initial temperatures and pressure

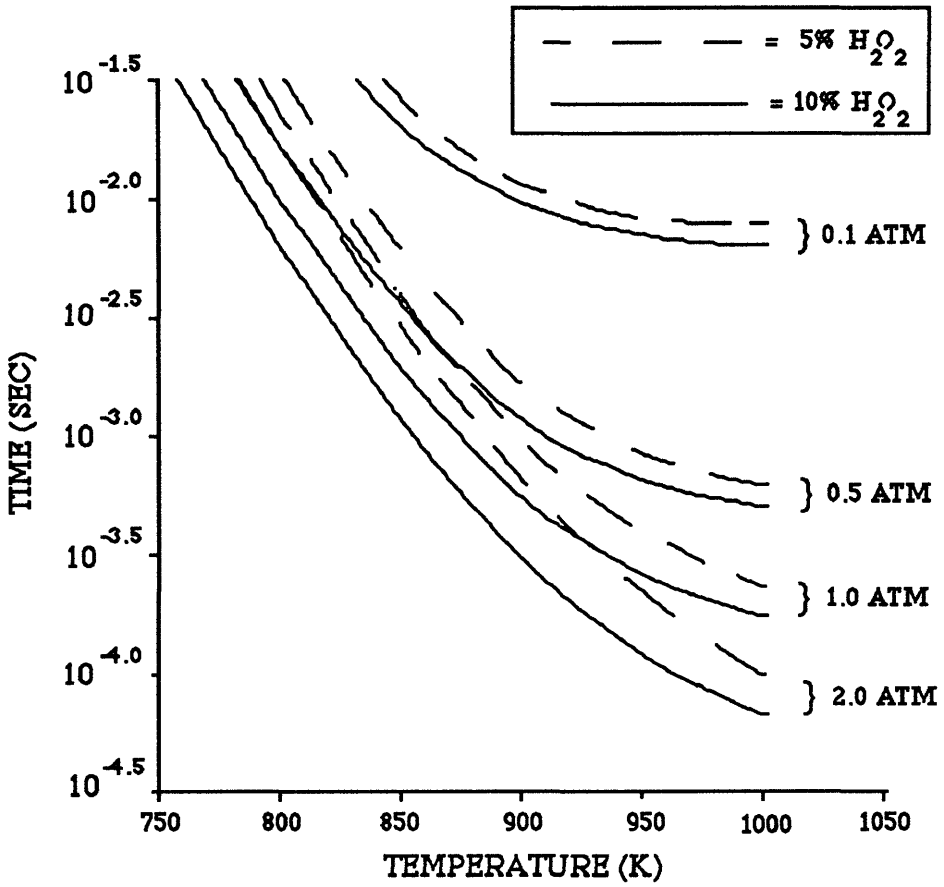

Figure 4.9: Effect of hydrogen peroxide as a function of temperature for T<1050 K

the silane will ignite. If the temperature rise associated with the silane combustion is sufficient, the hydrogen will begin combustion.

The reaction mechanism was assembled from the data for References [17] and [18]. Table A.5 (see Appendix A) contains the reaction mechanism and Arrenhius rate constants. These reactions are in addition to the basic H_2-air system of Table A.3.

Figure 4.10 plots the total reaction time versus initial temperature and pressure for a mixture of stoichiometric hydrogen and air plus 2.5% mass fraction silane. As seen in the figure, the nonlinearity in the 900 K and 1000 K lines are almost completely erased. The ignition limit has been overcome by raising the temperature through the initial combustion of silane.

Figure 4.11 shows the effect of varying the mass fraction of SiH_4. Similar to the hydrogen peroxide case, the mixtures initially affected by the ignition limit (dotted lines in the figure) experiences drastic decreases in total reaction times. Most of the decrease in reaction times occurs for silane addition accounting for mass fractions less than 2.5%.

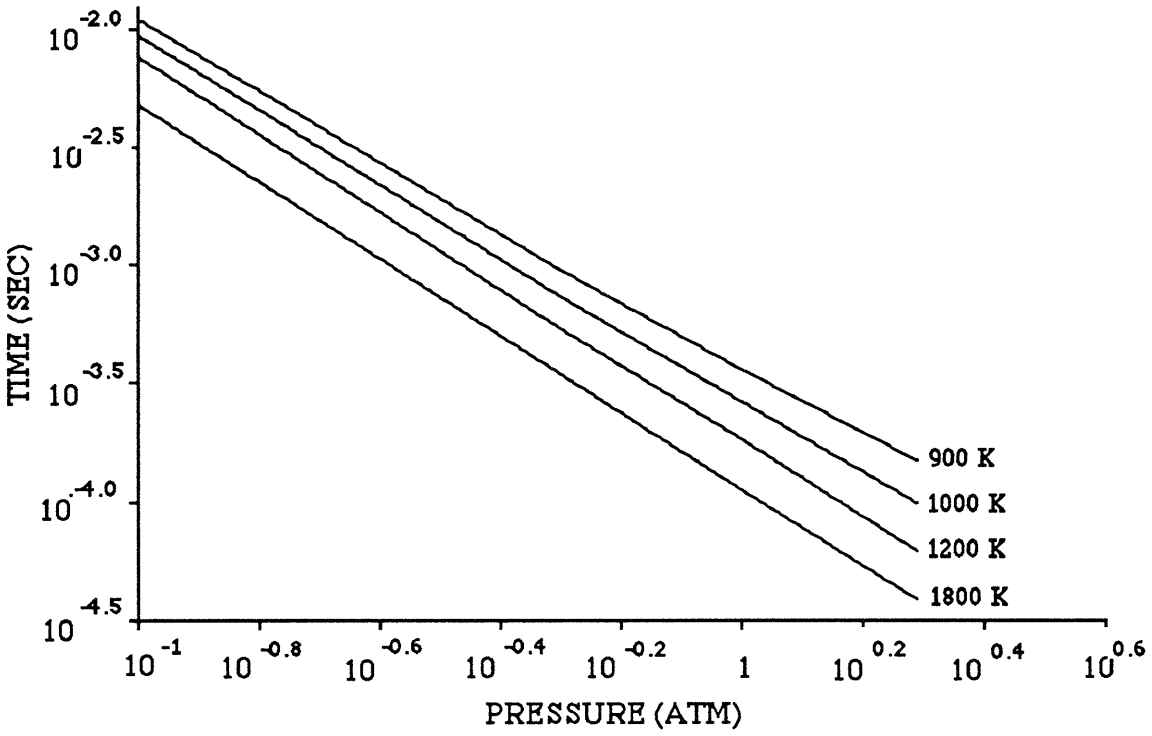

Figure 4.10: Total reaction times for the H_2-Air-2.5% mass fraction SiH_4 system as a function of initial temperature and pressure.

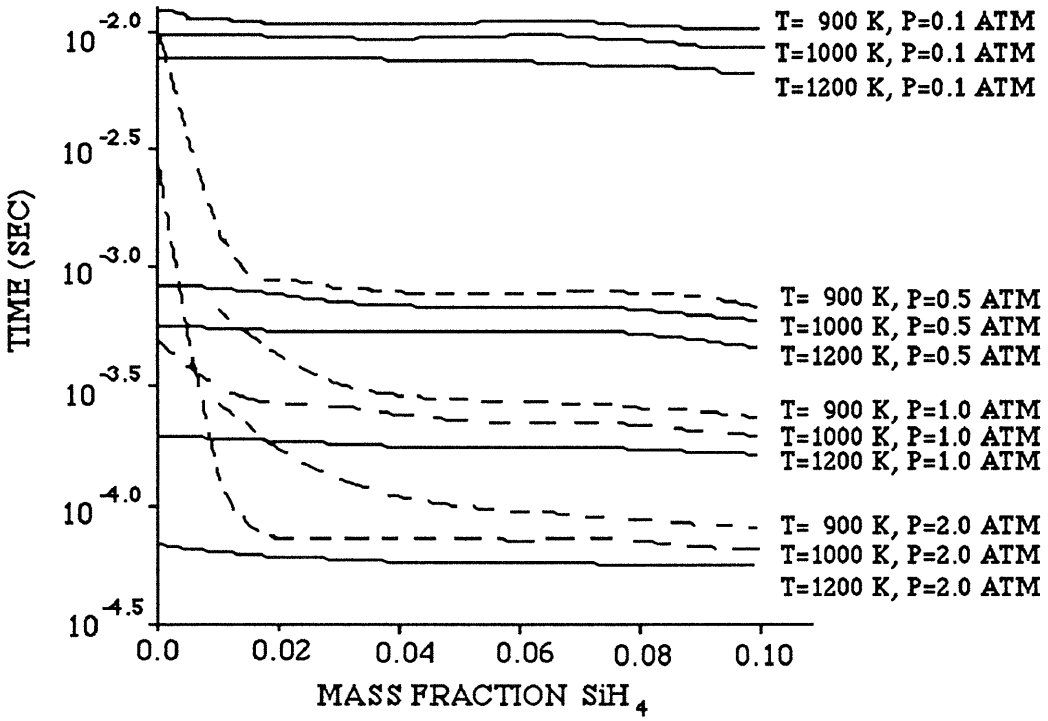

Figure 4.11: Effect of increasing SiH_4 on the reaction time. Drastic reductions in reaction time occur for points above the ignition limit of H_2 (dotted lines). More moderate reductions occur at other temperatures and pressures.

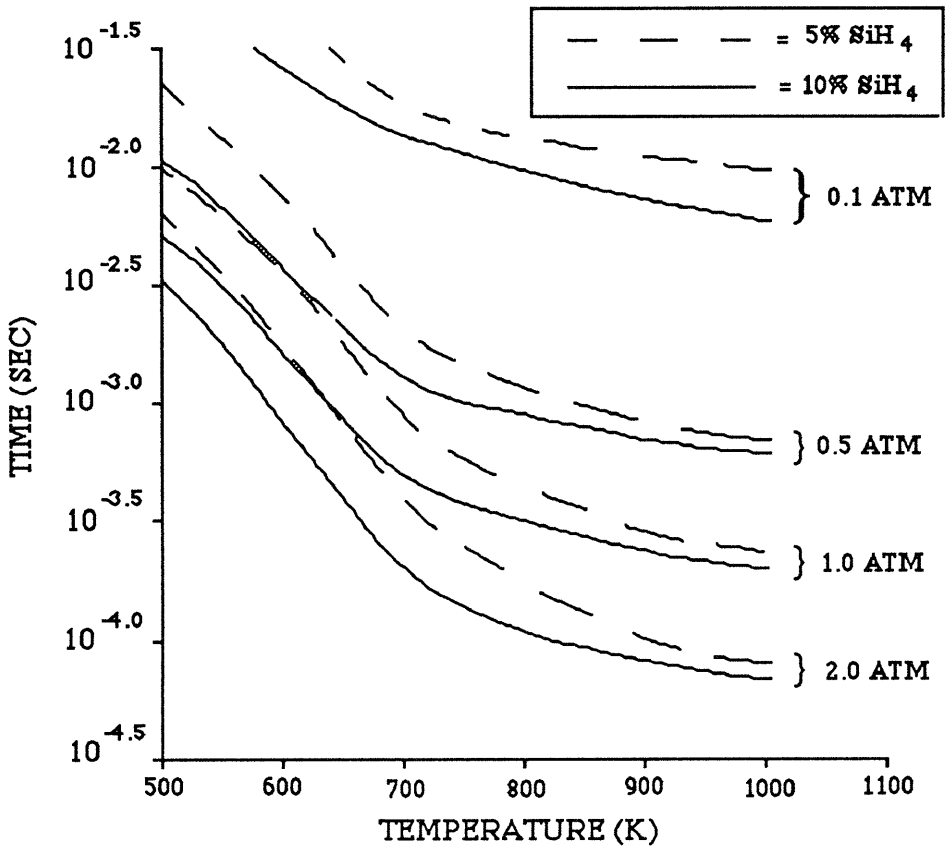

Figure 4.12: Total reaction times for mixtures containing 5% and 10% mass fraction silane as a function of temperature and pressure

More moderate decreases are noted for further silane addition. For temperatures and pressures not effected by the ignition limit, slight decreases in reaction time occur with increased amounts of silane.

The effect of adding silane at temperatures below 1000 K was also studied (see Figure 4.12). Ignition is achieved over the entire temperature range considered ($500K < T < 1000K$). To maintain total reaction times of approximately 1.0 ms, however, the pressure must still be maintained at above approximately 0.5 atm. Below this, the reaction times necessary to achieve silane combustion increase substantially.

Similar to Figure 3.2, Figure 4.13 is a contour plot of the required combustor length for complete combustion at the first design point. For this figure, 5% mass fraction silane was added for all flight Mach numbers below 10. The constraint on the lower Mach number flight caused by the ignition limit is removed. Combustion lengths around 1.0 m may now be maintained down to M=5 as long as the pressure is kept above about 1.0 atm.

Figure 4.14 presents the combustor lengths needed for the second design point. Here, 5% mass fraction silane was added for all flight Mach numbers below 12.5. For this

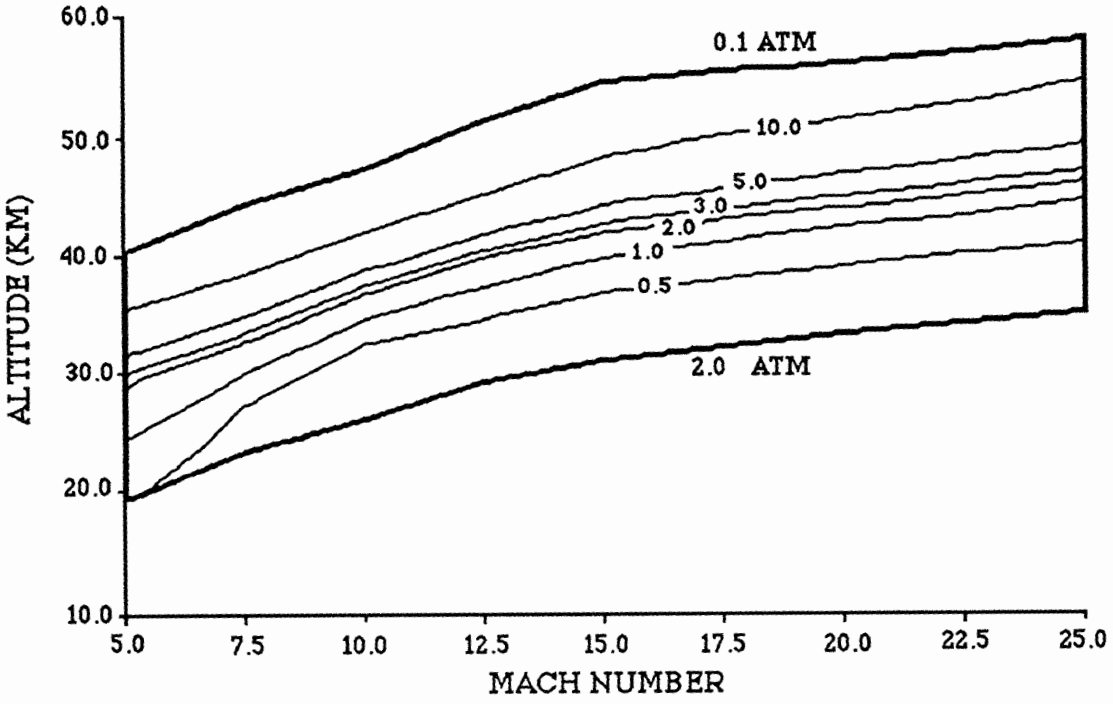

Figure 4.13: The effect of 5% silane on the lengths required for total combustion. Design point 1

design point, the required combustor length still exceeds 10 m at a flight Mach number of 5. For comparison, Figure 4.15 also shows the required combustor lengths for the second design point. For this figure, 10% mass fraction silane has been added for all flight Mach numbers below 12.5. Increasing the mass fraction of silane provides only a small further advantage.

Although quite effective in enhancing ignition in the H_2 system, silane has several serious drawbacks. First is the danger in handling and transporting silane. In addition to being violently reactive in contact with air at room temperatures, silane is highly toxic. The recommended toxicity level is 5 ppm [19], half that of hydrogen cyanide. Second, the products of silane combustion are SiO and SiO_2. The SiO_2 formed in the combustor will quite likely be above its vapor pressure: condensation is likely to occur [20]. Indeed, in the report on the ground based tests, Diskin and Northam [21] state that a film of deposited SiO_2 covered the engine after silane was used as an ignition aid. The effect of SiO_2 contamination on the vehicle will need to be thoroughly understood before silane is used in an actual flight vehicle.

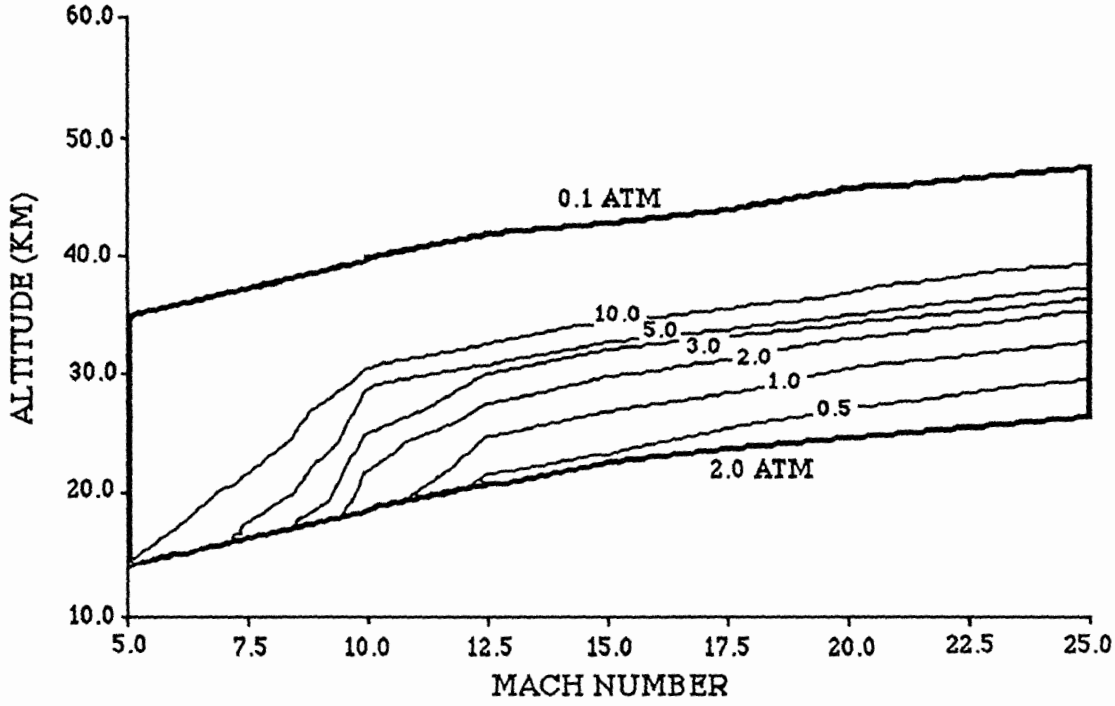

Figure 4.14: The effect of 5% silane on the lengths required for total combustion. Design point 2.

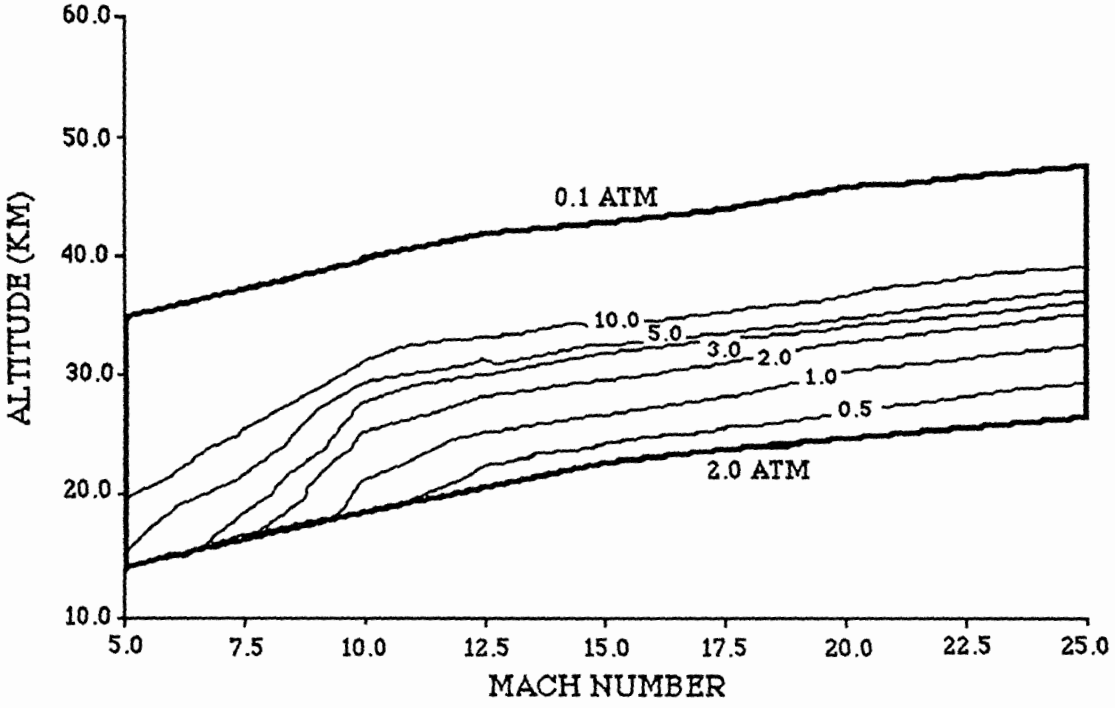

Figure 4.15: The effect of 10% silane on the lengths required for total combustion. Design point 2

Chapter 5

Nozzle Results

As pointed out in the introduction, the nozzle of the proposed hypersonic vehicle is actually the entire aftbody of the aircraft. The interaction of the exhaust from the SCRAMJET with the aftbody and freestream will make the nozzle configuration highly dependent on three-dimensional effects. In addition, potentially serious performance losses are possible if the dissociation energy of free radicals in the flow exiting the SCRAMJET is not regained as kinetic energy in the nozzle.

A highly simplified but still useful one-dimensional model of the nozzle flow is to consider the nozzle as a simple conic expansion, much like a rocket nozzle. In this model, two limiting cases can be investigated along with the exact kinetic solution. The "frozen" solution, in which no chemical reactions occur and all dissociation is lost, is the worst case. On the other hand, if the flow remains in equilibrium at all points, the greatest amount of dissociation energy is regained. The equilbrium solution then provides the best possible limit.

One of the underlying differences between the equilibrium, frozen and kinetic solutions involves the length scales inherent in the problem formulation. The frozen and equilibrium solutions are isentropic and do not involve a streamwise length scale. For these solutions, the flow properties are functions only of cross-sectional area and are independent of the expansion rate of the nozzle. The kinetic solution, however, does have a streamwise length scale, and the solution will be dependent on the expansion rate. This will be investigated below.

In order to estimate the performance losses incurred from incomplete recombination in the nozzle, three performance parameters are introduced. These parameters involve the total impulse, I:

$$I = \dot{m}\,u + P\,A \tag{5.1}$$

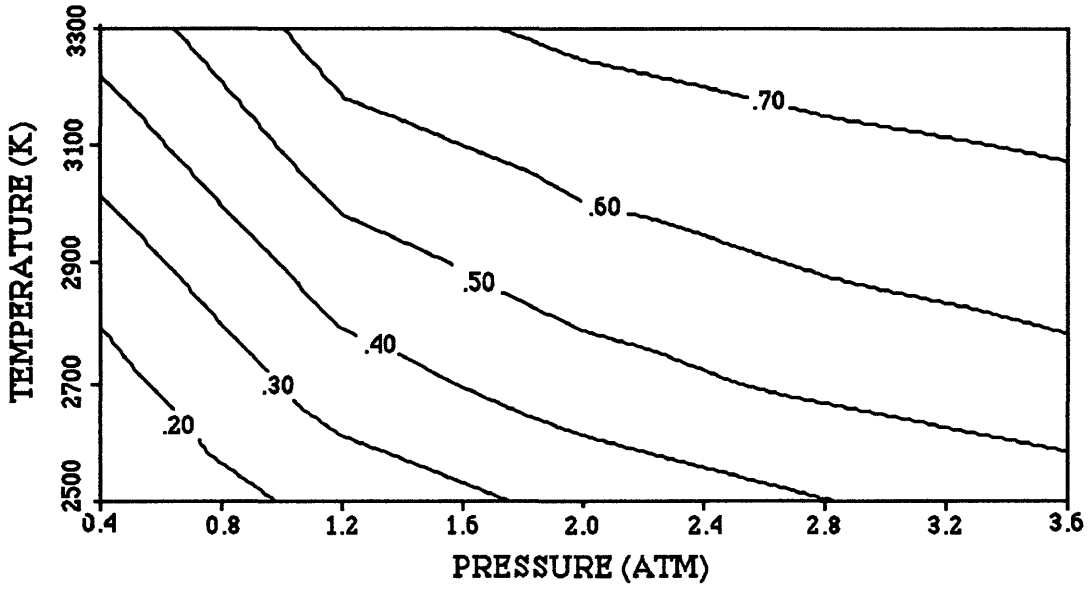

Figure 5.1: ϕ vs initial pressure and temperature for an initial velocity of 5500 m/s and 12.5 degree half angle conical expansion

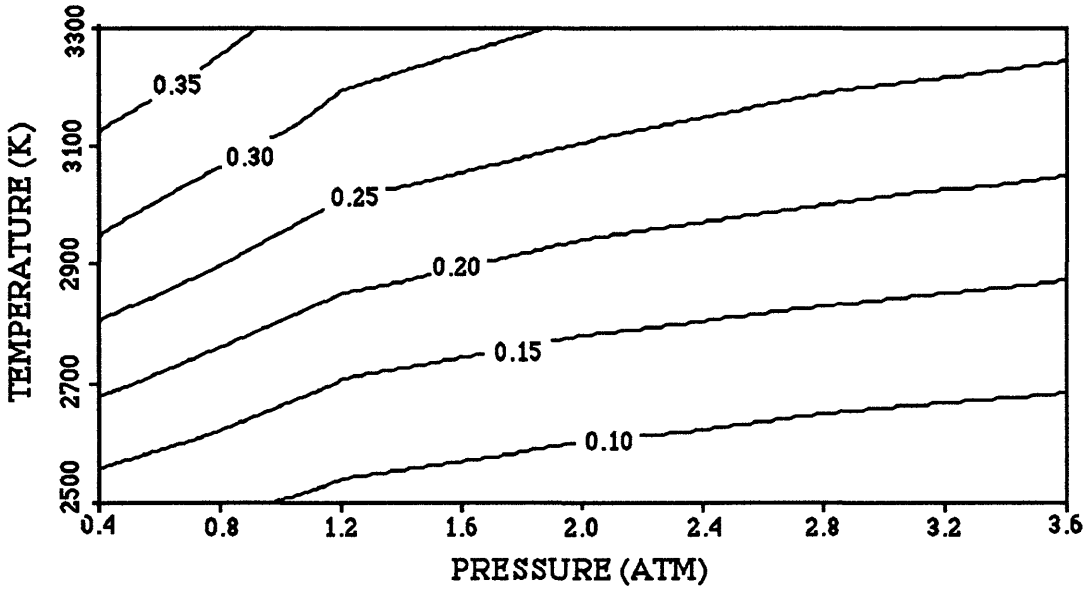

Figure 5.2: τ as a function of pressure and temperature for an initial velocity of 5500 m/s

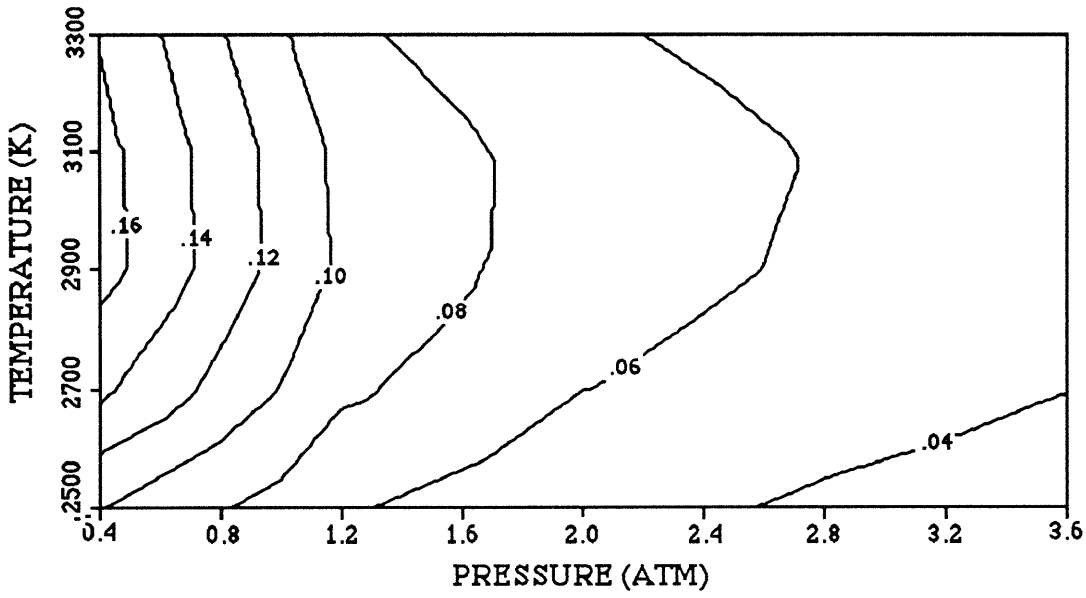

Figure 5.3: ζ as a function of pressure and temperature for an initial velocity of 5500 m/s

where u is the velocity, P is the static pressure and A is the cross-sectional area. For a given area expansion ratio, the value of I may be found for the equilibrium, kinetic, and frozen solutions (denoted by I_e, I_k, and I_f respectively).

To estimate the absolute effect of the energy entrained as dissociation energy at the combustor exit, the parameter τ is defined as

$$\tau \equiv \frac{I_e - I_f}{I_f - I_{initial}} \tag{5.2}$$

This parameter represents the difference between the impulse provided by the equilibrium and frozen solutions normalized by the total increase in impulse in the frozen solution. Essentially, τ provides a means of comparing the initial energy entrained as dissociation energy with the initial total energy of the flow exiting the combustor. If much of the flow's total initial energy is in the form of dissociation energy, τ will be relatively large.

The second parameter represents the fraction of the impulse "recovered" in the kinetic solution and is defined as

$$\phi \equiv \frac{I_k - I_f}{I_e - I_f} \tag{5.3}$$

A completely frozen nozzle will have $\phi = 0$ while a nozzle in equilbrium gives $\phi = 1$.

Table 5.1: Numbering system of lines on the following figures

Line Number	Initial Pressure (atm)	Initial Temperature (K)
1	0.4	2500
2	0.4	2900
3	0.4	3300
4	2.0	2500
5	2.0	2900
6	2.0	3300
7	3.6	2500
8	3.6	2900
9	3.6	3300

Finally, the previous two parameters can be combined into a third parameter, ζ. The definition of ζ is

$$\zeta = \frac{\tau}{1+\tau}(1-\phi) = \frac{I_e - I_k}{I_e - I_{initial}} \tag{5.4}$$

ζ provides an overall measure of the freezing losses in the nozzle by normalizing the difference in the equilibrium and kinetic impulses by the total increase in equilibrium impulse.

To investigate the performance of the nozzle, ϕ ,τ and ζ are calculated below as a function of initial temperature and pressure in the nozzle for a fixed geometry. The initial velocity, area expansion ratio, and nozzle geometry are then parametrically varied to study the effect on the performance parameters. The following paragraphs discuss the results.

Figure 5.1 shows the parameter ϕ as a function of initial temperature and pressure for an initial velocity of 5500 m/s. The expansion is assumed to occur through a 12.5 degree half angle conical nozzle with an initial area of 1.0 m^2:

$$A = (1 + .28679\,x)^2 \tag{5.5}$$

to an area ratio $A/A_0 = 40$. At low initial temperatures and pressures, the recombination reactions are relatively slow. In this case, the kinetic solution is close to the frozen solution, and ϕ is small. As seen in the figure, for an initial temperature of 2500 K and initial pressure of 0.4 atm, less the 20% of the impulse is "recovered". For increasing temperature, the reactions are faster. Increasing pressure also makes the third body reactions more effective. Then, for both increasing initial temperature and pressure, the

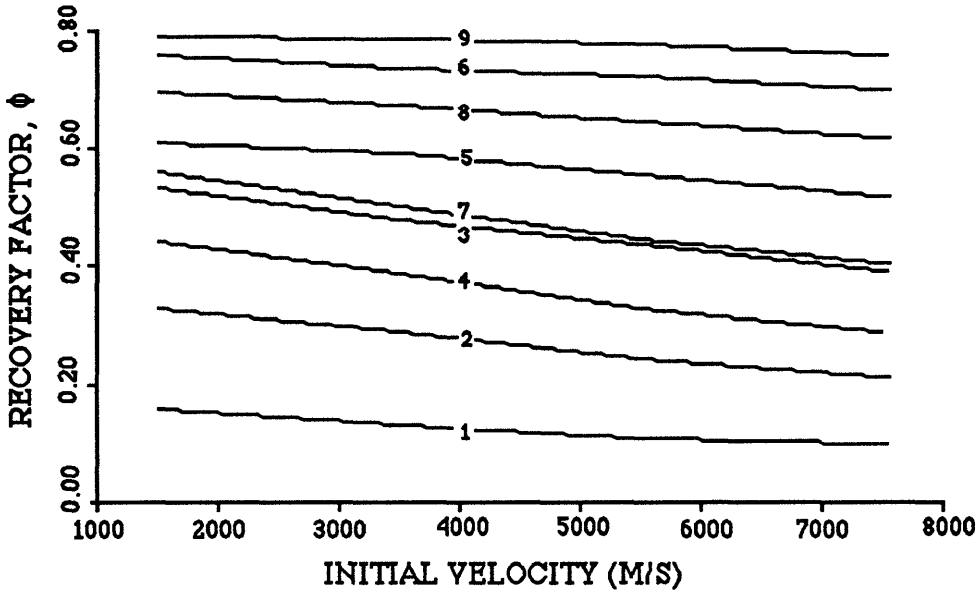

Figure 5.4: Effect of velocity on ϕ. The plot is for A/A_0 =40 for a 12.5 degree half-angle conic section. See Table 5.1 for key to line numbers.

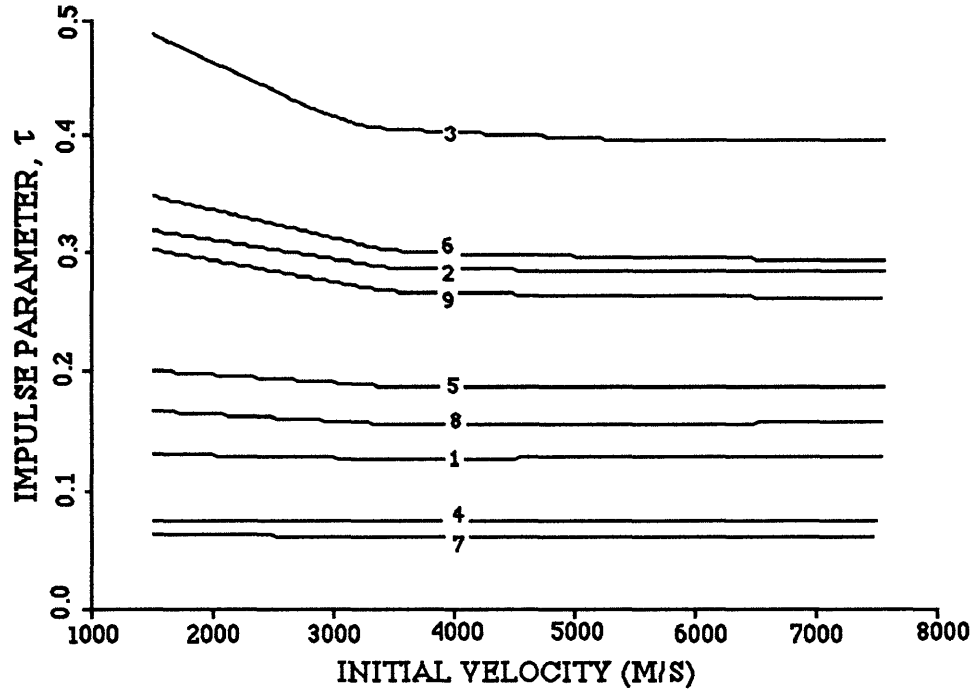

Figure 5.5: Effect of velocity on τ. The plot is for $A/A_0 = 40$ for a 12.5 degree half-angle conic section. See Table 5.1 for key to line numbers.

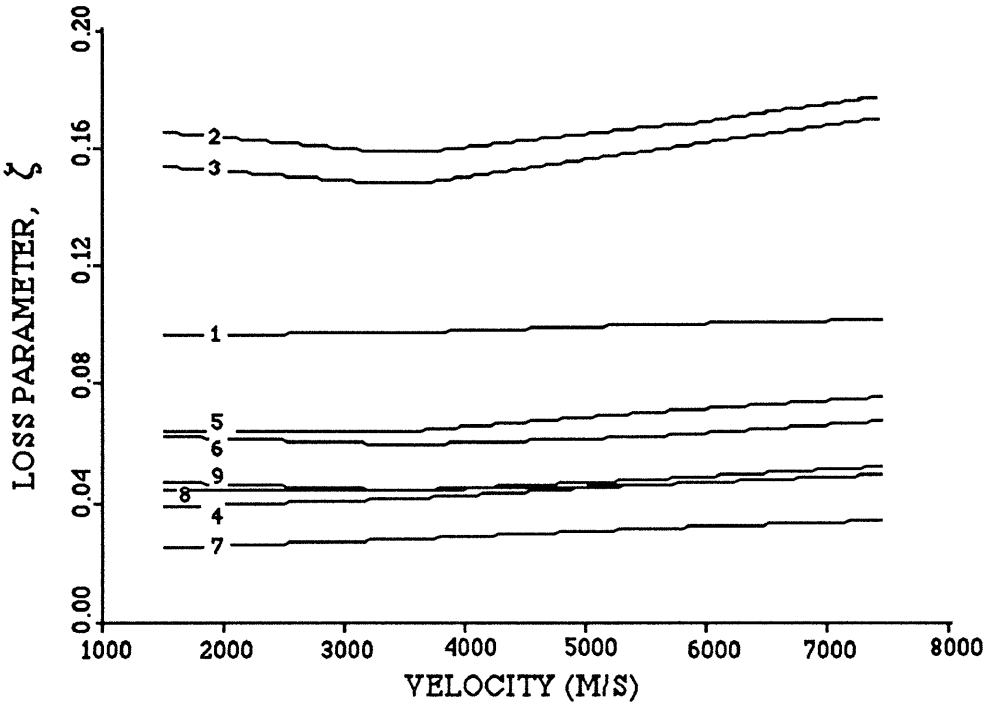

Figure 5.6: Effect of velocity on ζ. The plot is for $A/A_0 = 40$ for a 12.5 degree half-angle conic section. See Table 5.1 for key to line numbers.

kinetic solution should tend toward the equilibrium solution, and the amount of recovered impulse should increase. This is seen in the figure as the amount of impulse recovered increases roughly along the diagonal and exceeds 70% at 3300 K and 3.6 atm.

Figure 5.2 shows the absolute effect of the chemistry as a function of initial temperature and pressure for an initial velocity of 5500 m/s. The amount of energy stored as dissociation energy at the beginning of the nozzle is highly dependent on the temperature and weakly related to the pressure. The initial potential energy in the flow is related to the initial pressure. At low temperatures and high pressures, the amount of dissociation energy is small and the amount of potential energy is large. The fraction of dissociation energy to the total energy of the flow should be small. In this case, the difference between the equilibrium and frozen solution and , ultimately, the parameter τ should also be small. This is clearly shown in the figure with τ being less than 10% at an initial temperature of 2500 K and pressure of 3.6 atm. The fraction of energy stored as dissociation energy should increase with increasing temperature and decreasing pressure. Again, this is clearly seen in the figure as τ increases along the diagonal, exceeding 35% at an initial temperature of 3300 K and an initial pressure of 0.4 atm.

Figure 5.3 illustrates the overall performance loss in the nozzle. As discussed in the previous paragraphs, for a given pressure, increasing temperature causes an increase in the impulse "recovered" . Increasing temperature also causes an increase in the absolute difference between the equilibrium and finite rate impulses. Both τ and ϕ increase with increasing temperature for a given pressure. The combination of τ and ϕ, as represented by ζ, however, shows a maximum performance loss to occur. Referring to Figure 5.3, the maximum loss in performance occurs at about 3100 K for any given pressure. Because more of the dissociation energy is recovered at higher pressures, the overall performance loss also decreases with increasing pressure for any given temperature. In the worst case (low pressure at about 3100 K), the value of the loss parameter is slightly over 0.16.

The effect on ϕ of parametrically varying the initial velocity is investigated in Figure 5.4. The different lines represent different various initial temperatures and pressures (see Table 5.1 for key to line numbers). The results are plotted for an expansion ratio A/A_0 = 40 through a 12.5 degree half-angle conic section. The parameter ϕ is seen to be reasonably independent of the initial velocity, with slight reductions occurring with increased initial velocity. As velocity increases, the flow has a shorter residence time in which to equilibrate, hence the reduction in ϕ. Also with increasing velocity, the energy of dissociation represents a slightly smaller fraction of the total energy in the flow since the initial kinetic energy is increasing. The parameter τ should therefore decrease with increasing initial velocity (see Figure 5.5 and again refer to Table 5.1 for the key to the different lines which represent different initial conditions). The decrease in τ is most noticeable at high temperatures and low pressures where the dissociation energy is greatest. Combining ϕ and τ again provides an estimate of the overall performance loss in the nozzle (see Figure 5.6). In this case, ϕ and τ both slightly decrease with increaseing velocity. This is reflected in the slight minimums that occur in ζ. The minimum is most noticeable at low pressures and high temperatures (lines 2 and 3 of Figure 5.6). For the low pressure cases, ζ is about 0.15 while for higher pressure cases, ζ is approximately 0.05.

Figures 5.7, 5.8 and 5.9 show the effect of parametrically varying the area ratio. The initial velocity is 5500 m/s, and the expansion again occurs through a 12.5 degree half-angle conic section. Since the flow is expanding through the nozzle, varying the area ratio is equivalent to considering the flow at different positions of x. Two distinct trends exist for ϕ. For high initial temperatures (lines 3, 6 and 9 on Figure 5.7), ϕ slowly decreases with increasing area ratio. In comparison, for lower initial temperatures (lines 1, 4 and 7), ϕ increases with increasing area ratio.

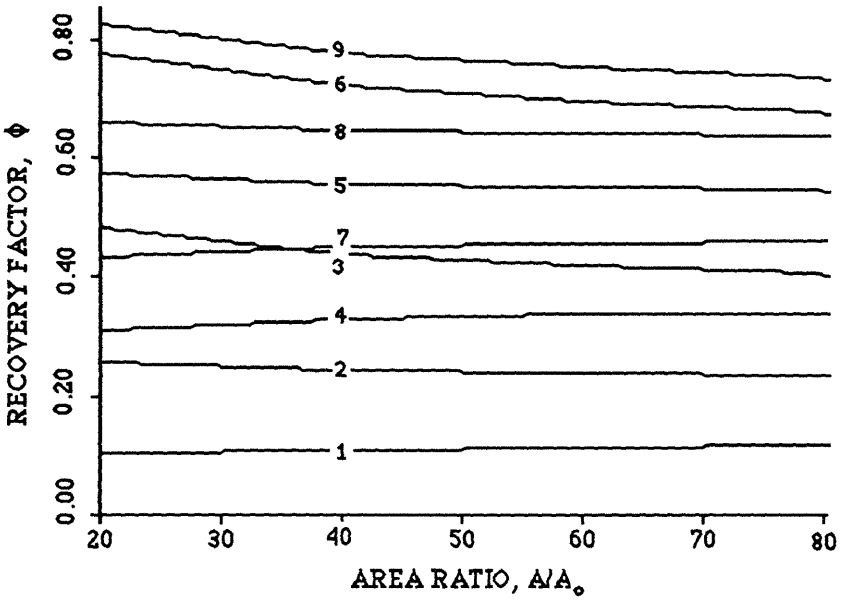

Figure 5.7: Effect of area ratio on ϕ. The plot is for expansion in a 12.5 degree half-angle conic section. See Table 5.1 for key to line numbers.

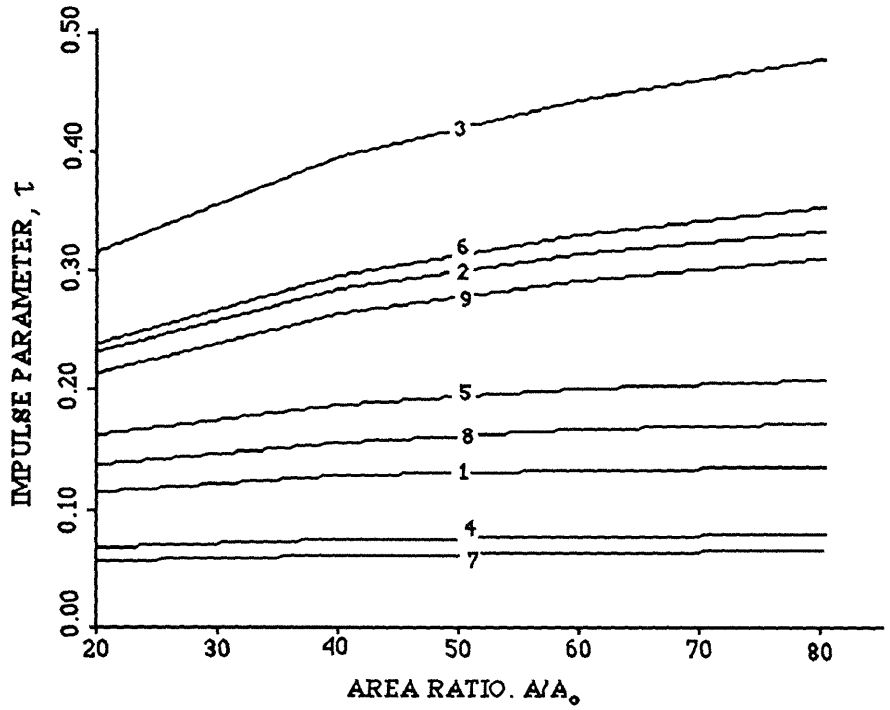

Figure 5.8: The effect of area ratio on τ. The plot is for expansion in a 12.5 degree half-angle conic section. See Table 5.1 for key to line numbers.

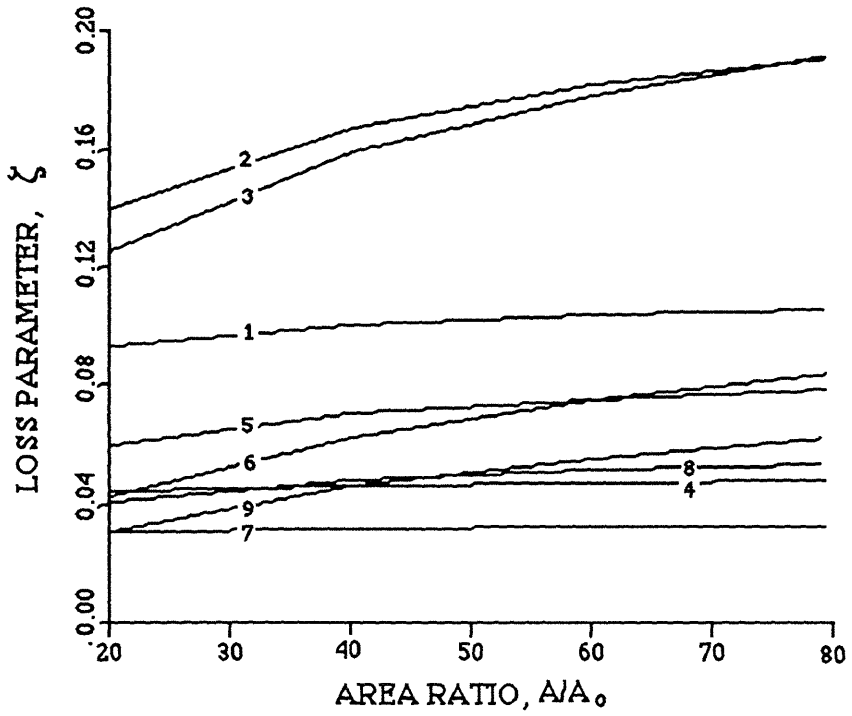

Figure 5.9: The effect of area ratio on ζ. The plot is for expansion in a 12.5 degree half-angle conic section. See Table 5.1 for key to line numbers.

Also, as the flow traverses the channel, dissociation energy is slowly converted to kinetic energy. The equilibrium and frozen solutions should slowly diverge. This is seen in Figure 5.8 as an increase in τ with increasing area ratio. The greatest increase in τ occurs for high temperature flows in which the initial dissociation energy is greatest.

Since τ increases with increasing area ratio and ϕ is roughly constant, the value of ζ increases with increasing area ratio (see Figure 5.9). The worst loss in performance again occurs for the low pressure cases (lines 1, 2 and 3). For these worst case situations, the value of ζ approaches 0.20. However, for most of the cases, the value of ζ is below 0.10.

Figures 5.10, 5.11, and 5.12 plot the relation between the nozzle half angle and the performance parameters. The half angle is extended beyond 35 degrees. Although the expansion rate shouldn't affect the equilibrium or frozen solutions, it will affect the kinetic solution. The 35 degree half angle is probably well beyond the applicable region of the 1-D model, but the solution is still shown since the trends with increasing nozzle half angle are apparent. As the half angle increases, the flow freezes faster. A decrease in ϕ should then accompany increasing half angle (see Figure 5.10). The largest decreases occur in the flow for which the dissociation energy is initially the greatest percentage of

the total energy. Finally, since I_f and I_e are both independent of expansion angle, the parameter τ should also be independent of the expansion angle. This is shown in Figure 5.11 and provides a nice confirmation of the model. With τ constant and ϕ decreasing with increasing nozzle half angle, ζ should increase with increasing half angle. This is shown in Figure 5.12. For the worst, low pressure cases (see lines 2 and 3), ζ reaches approximately 0.20. For all other cases, however, ζ is below 0.10.

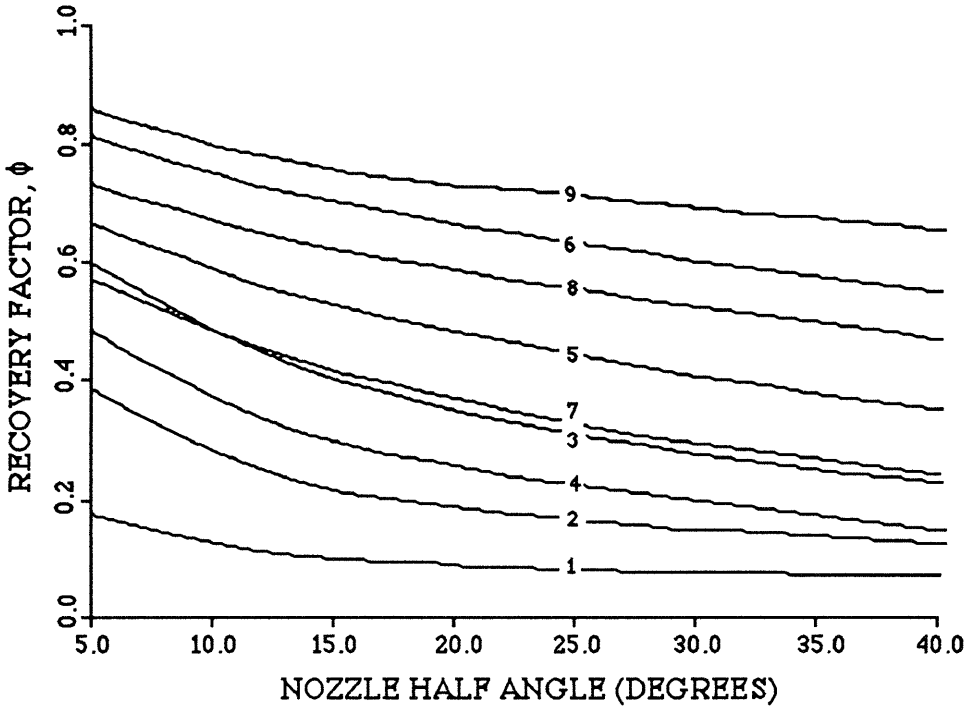

Figure 5.10: The effect of nozzle half angle on ϕ. See Table 5.1 for key to line numbers.

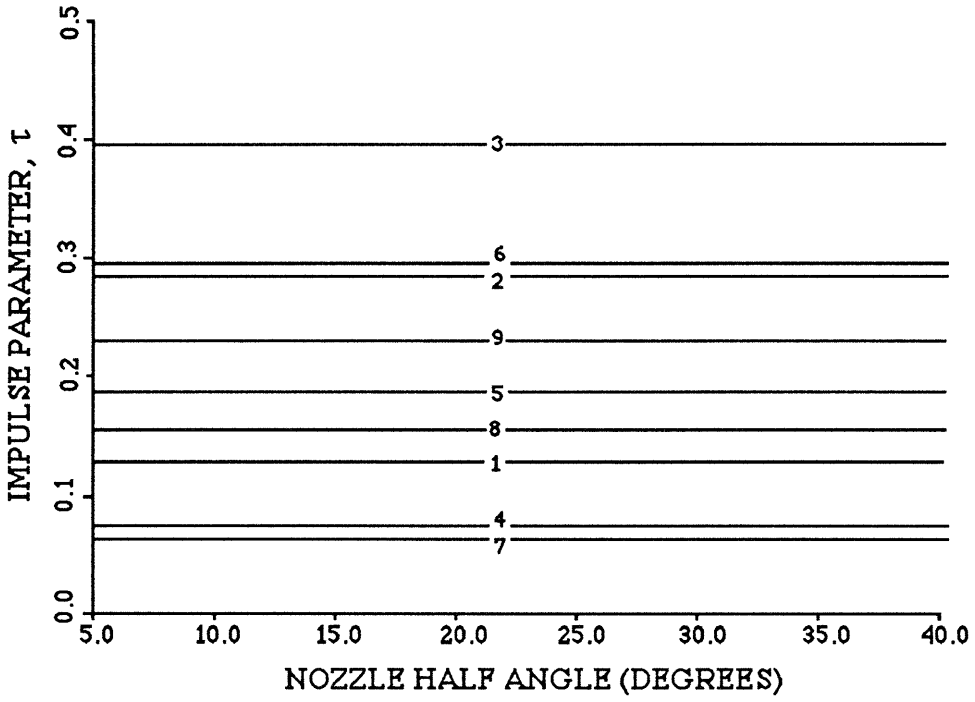

Figure 5.11: The effect of nozzle half angle on τ. See Table 5.1 for key to line numbers.

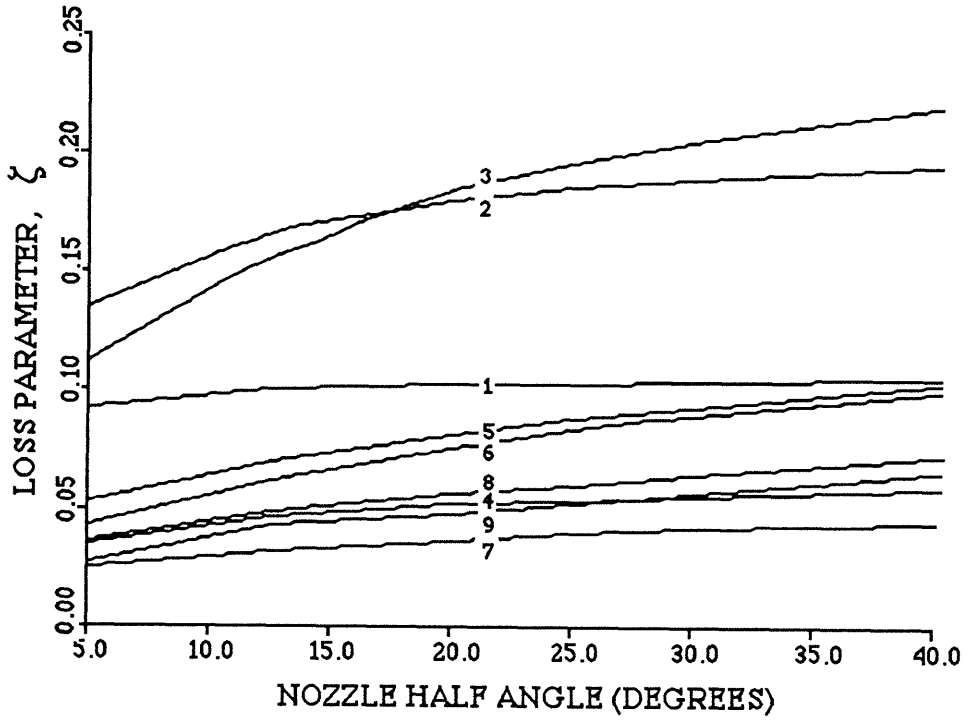

Figure 5.12: The effect of nozzle half angle on ζ. See Table 5.1 for key to line numbers.

Chapter 6

Vehicle Performance Results

The last three chapters have, in essence, considered the inlet, combustor, and nozzle as separate components. In this chapter, an attempt is made to integrate the models of the three components into a single estimate of the performance of the vehicle propulsion system. Once again, since the component models are clearly highly simplified, the goal here is not to present results that are precise indicators of an actual vehicle's performance but instead to estimate the possible losses incurred from the effects of chemical kinetics.

For this chapter, the independent variables are assumed to be the fuel addition pattern and area. The combustor consists of a 3 m long, conical, 5 degree half angle expansion with an initial area of 1 m^2:

$$A = (1 + .08749\,x)^2 \qquad for\ 0 < x < 3 \tag{6.1}$$

In the combustor, fuel injection occurs at two points: x=0.2 m and x=1.5 m. Eighty percent of the fuel is injected at the forward point with the remaining fuel injected at the aft point. At both points, the fuel is injected at the sonic velocity at 1000 K. Mathematically, the "step" functions are modelled as Fermi functions with and e-folding axial range of 2 cm:

$$f = .029\left[.80\left(\frac{1}{1 + \exp(-50\,(x - .2))}\right) + .20\left(\frac{1}{1 + \exp(-50\,(x - 1.5))}\right)\right] \tag{6.2}$$

The combustor is, of course, attached to the nozzle. Again, because of the inherent 3-D nature of the SCRAMJET nozzle, great difficulty is realized in applying the 1-D model. Typical pressures at the exit of the combustor require area expansion ratios on the order of 50:1 or greater in order to achieve perfect expansion at the design point. Assuming a conical expansion, a 12.5 degree half angle requires a length of nearly 30 m for such an area ratio. In comparison, a 10 m long nozzle requires about a 35 degree half angle. The first model, a 30 m long nozzle, is clearly far too large for an actual vehicle.

Unfortunately, the second model, while being a more reasonable scale, falls outside the range of applicability of the 1-D model. Luckily, the frozen and equilibrium limits are isentropic without streamwise length scales. As mentioned in the previous chapter, the equilibrium and frozen limit results are dependent only on expansion ratio and not on expansion rate. The kinetic solution, however, does have a streamwise length scale, and the solution will vary depending on the assumed expansion rate. As previously shown, however, the solution is not strongly dependent on the expansion rate. Therefore, for the present purposes, the 35 degree half angle model is chosen, and the errors in the 1-D model accepted. The area of the nozzle is

$$A = (1.5938 + .70021\,(x - 3))^2 \qquad for\ 3 < x \tag{6.3}$$

Figures 6.1 and 6.2 show the calculated specific impulse of the vehicle as a function of Mach number and altitude for the first and second design points, respectively. Both figures are for stoichiometric operation. For Figure 6.2, a 1% mass fraction of silane was added in order to achieve ignition for flight below Mach 10. Immediately noticeable on the figures is the fact that the assumption of rapid, step function fuel injection causes this design to choke for flight below approximately Mach 7.5. Below this Mach number, the propulsion system will act as a ramjet.

Just within the operational limit for the first design point, the specific impulse is almost 2700 s at the high pressure limit and 2400 s at the low pressure limit. The drop in I_{sp} with increasing altitude represents the increasing ratio of dissociation energy to total energy in the flow at the beginning of the nozzle. As shown below, the vehicle operates near the frozen limit. In the notation of the previous chapter, along the low trajectory, τ is large. Since the vehicle operates near the frozen limit, the dissociation energy is not regained (i.e. ϕ is small), and the performance losses increase. Along the lower, high pressure trajectory, τ is smaller. In this case, the performance losses are also smaller, and the specific impulse is correspondingly higher.

The specific impulse also drops dramatically with increasing Mach number. In fact, for high Mach numbers at the first design point, the specific impulse is negative. For this design point, at high Mach numbers, the stream entering the combustor is at a static temperature higher than the flame temperature of hydrogen. The injected hydrogen dissociates and cools the flow in the combustor. Initial energy from the flow is entrained as dissociation energy. This energy is not regained in the nozzle, and the specific impulse goes negative.

For the second design point, the specific impulse near Mach 7.5 is about 2500 s along

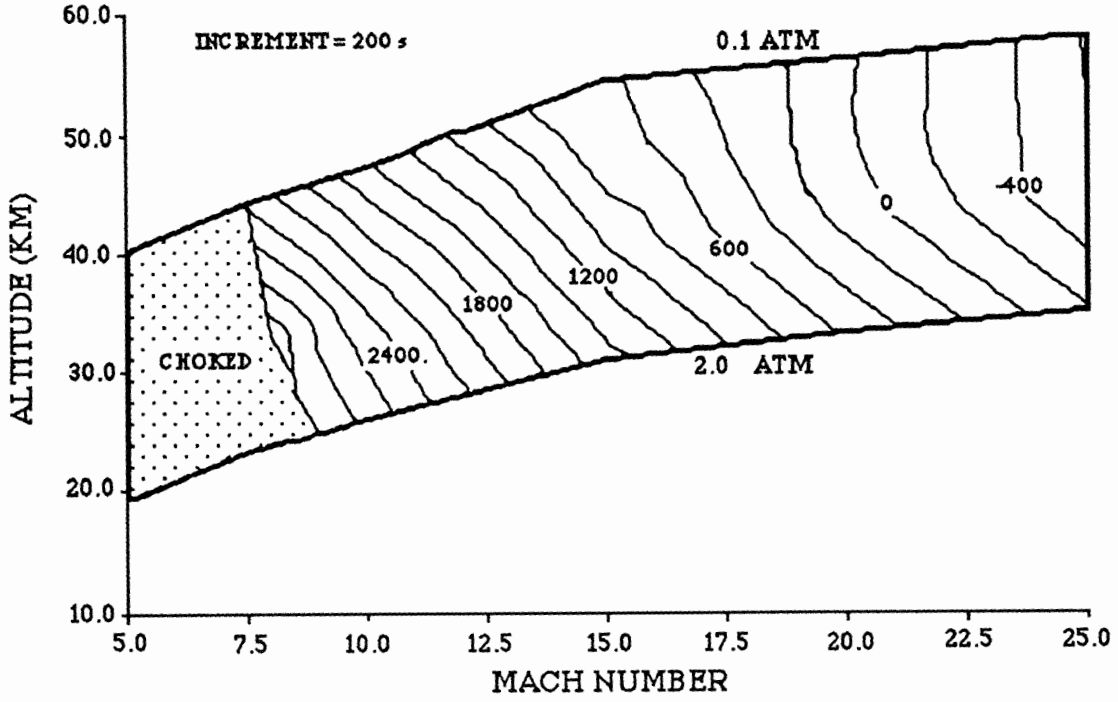

Figure 6.1: Specific impulse vs. Mach number and altitude for the first design point. The lines are lines of constant specific impulse, marked in seconds.

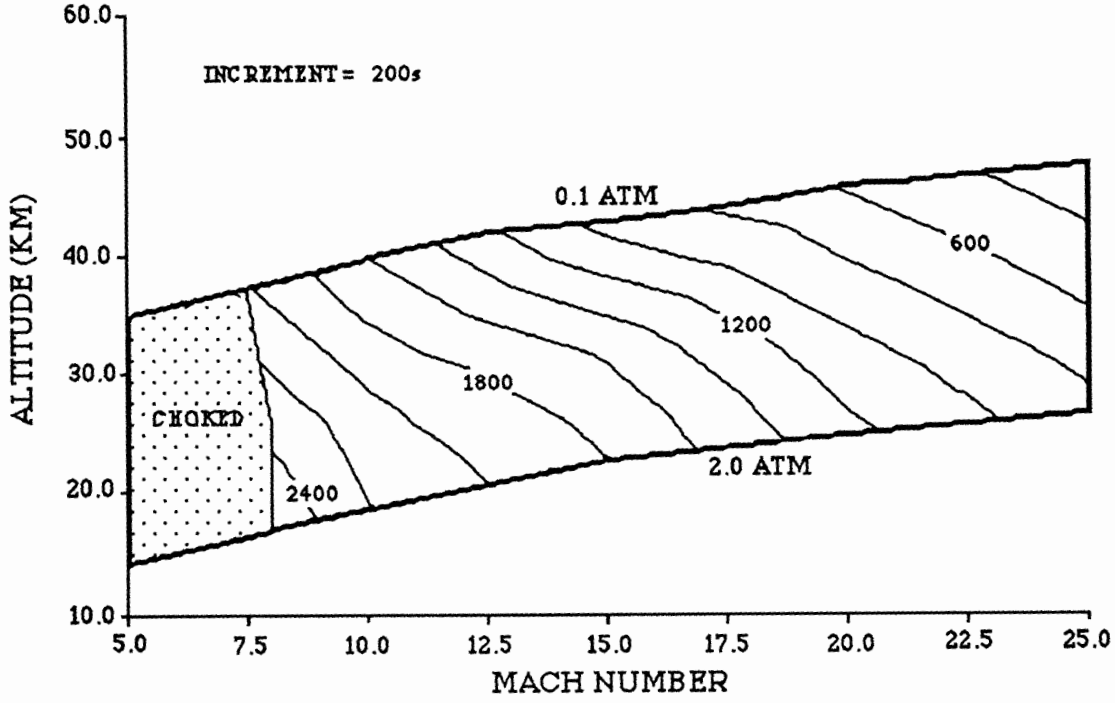

Figure 6.2: Specific impulse vs. Mach number and altitude for the second design point. The lines are lines of constant specific impulse, marked in seconds.

the low trajectory and falls to 2000 s at the upper trajectory. Increasing Mach number again causes the I_{sp} to fall rapidly. In this case, however, the initial static temperature never exceeds the flame temperature of hydrogen. The specific impulse remains positive throughout the flight corridor. At M=25, the specific impulse reaches 1000 s at the low trajectory but drops to under 300 s at the upper trajectory.

To better understand the losses due to the chemical kinetics, Figures 6.3 and 6.4 show the percentage of the equilibrium specific impulse lost in the kinetic and frozen solutions at the first design point. In Figure 6.3, the lines shown are lines of constant

$$\frac{I_{sp,eq} - I_{sp,ki}}{I_{sp,eq}} \tag{6.4}$$

Likewise, Figure 6.4 shows lines of constant

$$\frac{I_{sp,eq} - I_{sp,fr}}{I_{sp,eq}} \tag{6.5}$$

These two parameters are somewhat analogous to ϕ and τ of the previous chapter.

Figure 6.3 and 6.4 only include the data for Mach numbers at which the specific impulse remains positive.

As shown in Figures 6.3 and 6.4, the largest losses in I_{sp} on a percentage basis for both the frozen and kinetic solutions are incurred at high temperatures and low pressures (corresponding to a large values of τ in the notation of the previous chapter). This is the region in which the dissociation energy of the initial flow is the greatest percentage of the total energy. For the frozen flow, the dissociation is not regained as kinetic energy in the nozzle, so the high temperature, low pressure limit is also the region of the greatest performance losses. The similarity between Figures 6.3 and 6.4 also indicates the vehicle operates near the frozen limit for the entire flight envelope. At lower temperatures and pressures, more moderate reductions in I_{sp} are noted. Of course, the absolute value of specific impulse is smaller at the high temperature, low pressure limit, so absolute performance losses are not as great.

Figures 6.5 and 6.6 are similar to Figures 6.3 and 6.5. These figures, however, are for the second design point. With lower temperatures at the higher Mach numbers, the dissociation energy is smaller, so substantially smaller percentage losses occur. Percentage losses are restricted to under 80% at the high temperature, low pressure limit. Again, similarity between Figures 6.5 and 6.6 indicates the nozzle is operating near the frozen limit.

As briefly mentioned in Chapter 4, the vehicle may actually need to operate at an equivalence ratio greater than 1.0 in order to maintain a regenerative cooling capability.

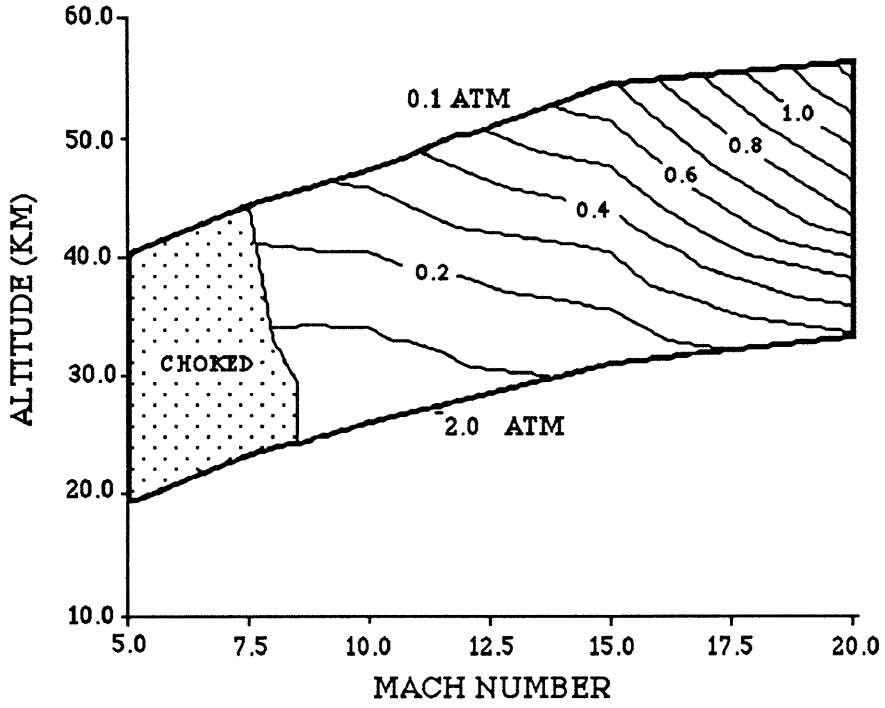

Figure 6.3: Penalty for kinetic solution for first design point. The lines marked are lines of constant $(I_{sp,eq} - I_{sp,ki})/I_{sp,eq}$.

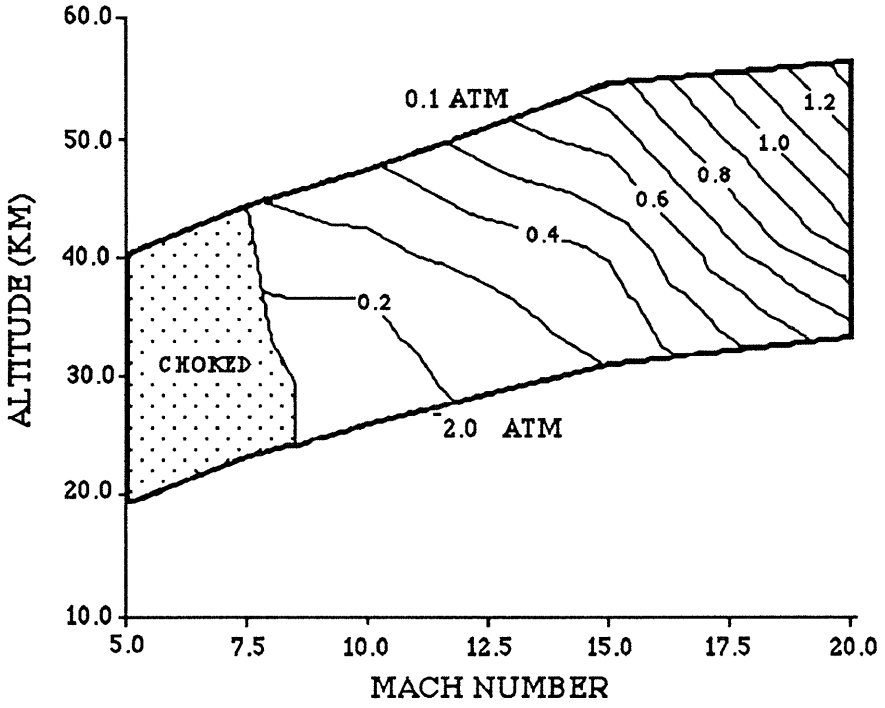

Figure 6.4: Penalty if nozzle were completely frozen for second design point. The lines marked are lines of constant $(I_{sp,eq} - I_{sp,fr})/I_{sp,eq}$

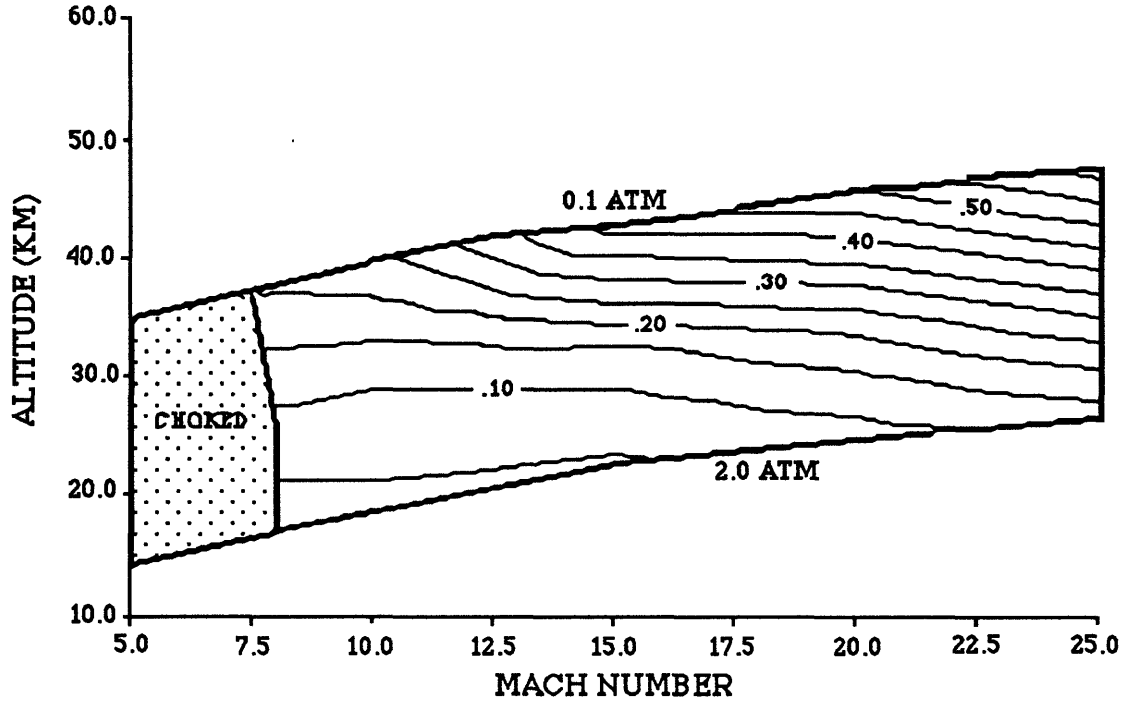

Figure 6.5: Penalty for kinetic solution for second design point. The lines marked are lines of constant $(I_{sp,eq} - I_{sp,ki})/I_{sp,eq}$.

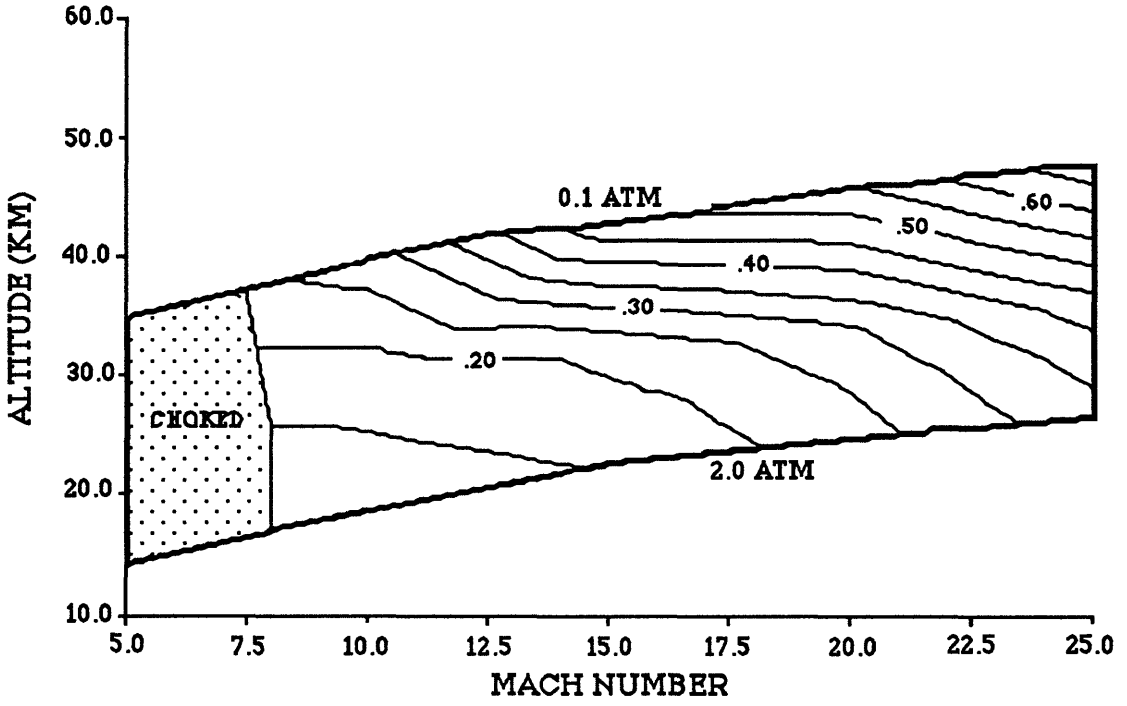

Figure 6.6: Penalty if nozzle were completely frozen for first design point. The lines marked are lines of constant $(I_{sp,eq} - I_{sp,fr})/I_{sp,eq}$

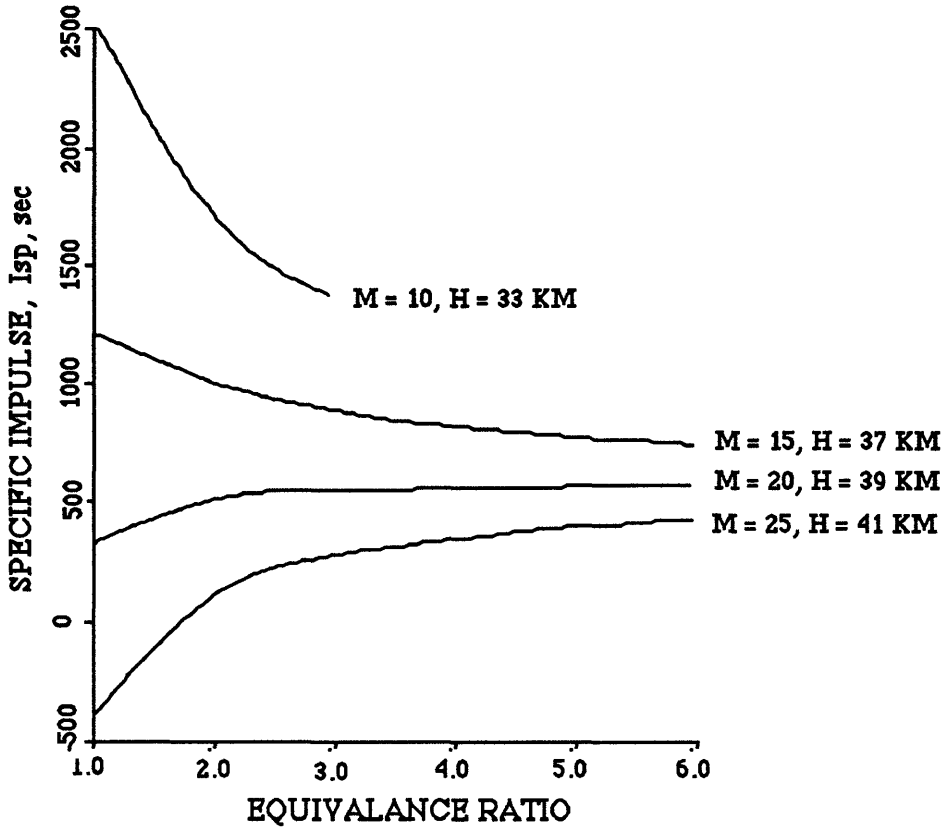

Figure 6.7: Specific impulse vs. equivalance ratio for various flight conditions. Design point 1.

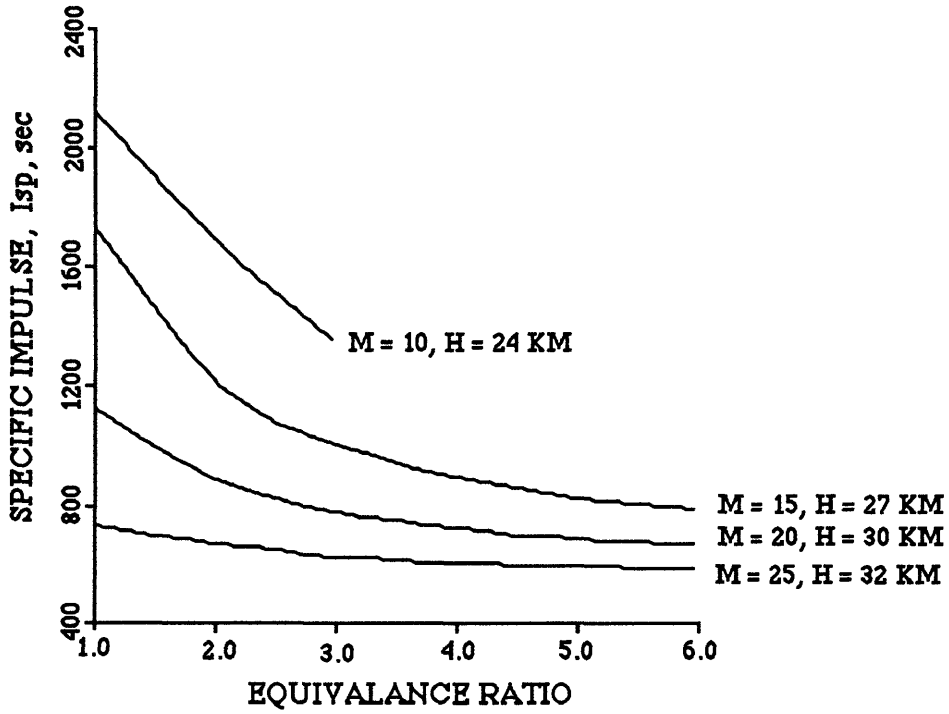

Figure 6.8: Specific impulse vs. equivalance ratio for various flight conditions. Design point 2.

The specific impulse for a vehicle operating at equivalence ratios greater than 1.0 is shown in Figures 6.7 and 6.8 for the first and second design points, respectively. The plots illustrate the behavior of the specific impulse as a function of equivalence ratio for several different flight conditions.

In Figure 6.7, the specific impulse at Mach 10 and 15 decreases with increasing equivalence ratio (the Mach 10 line is shortened by the choking of the engine at an equivalence ratio slightly greater than 3.0). The specific impulse at Mach 20 and 25, however, increases with increasing equivalence ratio. In all cases, the specific impulse nears an asymptote at slightly over 500 s.

The asymptote in Figure 6.7 is the specific impulse that would be obtained if the vehicle were to operate at an 'infinite' equivalence ratio. In this limit, the incoming airstream and heat release from combustion have negligible affects on the performance of the vehicle. The vehicle becomes a rocket, the 'fuel' of which is H_2 at the injection conditions. By using the assumed injection conditions of the H_2 and the known expansion ratio in the scramjet and nozzle, a simple isentropic expansion calculation (ignoring the effects of pressure mismatch at the nozzle exit) provides the limiting specific impulse of the hypothetical H_2 rocket. This calculation gives a limiting specific impulse of 530 s, which agrees well with the asymptote in Figure 6.7. Since the incoming airstream doesn't affect the performance of the vehicle in this limit (and since the pressure mismatch of the nozzle is ignored), the limiting specific impulse must be independent of the flight conditions.

For the Mach 10 and 15 lines of Figure 6.7, the combustion process releases substantial energy (represented by the relatively high specific impulses at an equivalence ratio of 1.0). 'Dumping' fuel into the flow at equivalence ratios greater than 1.0 adds the same total enthalpy to the flow, but the chemical energy is not released through chemical reaction. Since less energy is released per unit mass injected, the specific impulse decreases towards the H_2 rocket limit as the equivalence ratio is increased. At Mach 20 and 25, the temperature of the airstream entering the combustor is higher than the flame temperature of hydrogen. In these cases, at an equivalence ratio of 1.0, the injected fuel is simply dissociated, and the airstream is cooled (see the discussion of Figure 6.1 above). In this case, the injected H_2 never combusts. Injecting further H_2 into the airstream then further increases the total enthalpy. Increased total enthalpy of the flow is in turn related to increased thrust which increases the specific impulse. For Mach 20 and 25, then, the specific impulse of the vehicle increases with increasing equivalence ratio.

In Figure 6.8, trends similar to those of Figure 6.7 are observed. For this design point,

combustion of the injected fuel occurs over the entire trajectory. In all cases, the specific impulse decreases with increasing equivalence ratio. The lines again near an asymptote at slightly over 500 s, as they must since the limiting specific impulse, as discussed above, must be independent of the flight conditions.

Chapter 7

Conclusions

As stated in the introduction, the ultimate goal of this thesis is to suggest operational limits and estimate performance losses caused by chemical kinetic effects of the combustion process. Several major effects have been pointed out.

- Ignition Limitations

  As shown in Chapter 3, for temperatures below approximately 1000 K, the scavenging of free radicals during the formation of HO_2 inhibits the ignition of hydrogen. If the rate of scavenging exceeds the rate of formation of free radicals, the reaction reaches its ignition limit and stops. A comparison of the ignition limit of hydrogen with the conditions at the beginning of the combustor as a function of Mach number and altitude shows that limitations are placed on the vehicle at low Mach number. At low Mach number, the initial static temperature in the combustor is also low, and the hydrogen will not ignite. Depending on the geometry of the vehicle forebody, the ignition limit may be reached for flight below about Mach 12. Some type of ignition aid will be required over this portion of the trajectory. Although many possibilities exist for ignition aids, such as variable geometry, dump combustors, and flame holders, only fuel additives were investigated. Hydrogen peroxide offers an inexpensive possibility, but is limited to temperatures above 850 K. If temperatures fall below 850 K, another possible fuel additive is silane. Silane, which was used in subscale ground tests, provides ignition down to 500 K. Silane, however is expensive and dangerous. It's actual use in a flight vehicle may not be practical. The main conclusion to be drawn here is that a fixed geometry vehicle cannot sustain the required temperature range for effective hydrogen combustion over the entire trajectory without some type of ignition aid.

- Reaction Rate Limitation

  Comparison of the reaction times of the H_2-air system with the velocities through the SCRAMJET show the necessity of maintaining pressures on the order of 1.0 atm or higher in the combustor. For lower pressures, the third body reactions necessary to achieve full heat release become ineffective, increasing the length required for complete combustion.

  When combined with the inlet model, the reaction rate analysis shows that, to maintain sufficient pressure in the combustor, a trajectory must be flown that is much lower than that traditionally associated with a hypersonic vehicle. Although the question was not addressed here, such low trajectories are likely to cause aerothermal and aeroelastic problems on other parts of the aircraft.

  It should also be noted that the estimates of required combustor length are still "best" case estimates, since mixing effects have not been considered. Mixing will substantially increase the length required for complete combustion.

- Nozzle Performance Losses

  For high temperatures and low pressures at the exit of the combustor, the energy in dissociation is a substantial fraction of the total energy in the flow. If the energy is not regained as kinetic energy in the nozzle, substantial performance losses will result. The amount of dissociation energy recovered is also dependent on the initial temperature and pressure. For high initial pressure, the third body reactions are effective. Freezing in the nozzle is delayed and the nozzle performance nears the equilibrium limit. For lower pressures, the nozzle freezes rapidly, causing a substantial performance penalty.

- Vehicle Performance Losses

  Chapter 6 uses a single design geometry to predict the overall losses incurred in the propulsion system. Substantial losses occur at low pressure and high temperature in the combustor since the ratio of dissociation to total energy is large, and the nozzle runs near the frozen limit. Far smaller losses occur along a high pressure trajectory.

  High initial temperatures in the combustor also place a limitation on the vehicle performance. As the initial temperature in the combustor exceeds the flame temperature of H_2, the specific impulse goes negative. The injected hydrogen is cooling the flow by converting thermal energy into dissociation energy. The dissociation energy is then not recovered in the nozzle.

The recurring theme through all these conclusions is the necessity of maintaining combustor pressures of 1.0 atm or greater, since the specific impulse of the vehicle uniformly increases with increasing combustor pressure. The actual limitation on the combustor pressure will eventually be dictated by other aerothermal and aeroelastic considerations for other portions of the vehicle. The trade-offs between these concerns and increasing performance losses with decreasing pressure must be carefully considered in the final design of the vehicle.

Bibliography

[1] Northam, G. B. and Anderson, G. Y., "Survey of Supersonic Combustion Ramjet Research at Langley", NASA Langley Research Center.

[2] Peterson, R. H., " Hypersonic Aircraft: from X-15 to National Aero-space Plane", presented as The Sam Bloomfield Distinguished Engineer Lecture Series at Witchita State University, 1987.

[3] Newberry, C. F., Dresser, H. S., Byerly, J. W., and Riba, W. T., "The Evaluation of Forebody Compression at Hypersonic Mach Numbers", AIAA Paper 88-0479.

[4] Shapiro, Ascher H., *The Dynamics and Thermodynamics of Compressible Fluid Flow, V. 1*, John Wiley and Sons, 1953.

[5] Vincenti, W. G. and Kruger, C. H., *Introduction to Physical Gas Dynamics*, Robert E. Kreiger Publishing Co.,1965.

[6] Bussing, Thomas R., "Chemistry Associated with Hypersonic Vehicles", AIAA Paper 87-1292.

[7] Liepmann, H. W. and Roshko, A., *Elements of Gas Dyanamics*, John Wiley and Sons, 1957.

[8] Gordon, S., McBride, B., Heimel, S., and Ehlers, J., "Thermodynamic Properties to 6000° K for 210 Substances involving the First 18 Elements", NASA SP-3001, 1963.

[9] Wakelyn, N. T. and McLain, Allen G., "Polynomial Coefficients of Thermochemical Data for the C-H-O -N System", NASA-TM-X-72657, 1975.

[10] Esch, D. D., Siripong, A. and Pike, R. W., "Thermodynamic Properties in Polynomial Form for the Carbon, Hydrogen, Nitrogen and Oxygen System from 300 to 15000 K", NASA RFL-TR-70-3, 1971.

[11] Rogers, Clayton R. and Schexnayder, Charles J.,"Chemical Kinetic Analysis of Hydrogen-Air Ignition and Reaction Times", NASA TP-1856, 1981.

[12] Gordon S. and McBride B. J., "Calculations of Complex Chemical Equilibrium Compositions, Rocket Performance, Incident and Reflected Shocks, and Chapman-Jouguet Detonations", NASA SP-273, 1976.

[13] Gear, C. W., "The Automatic Integration of Stiff Ordinary Differential Equations", *Information Processing*, 1969.

[14] Gear, C. W., *Numerical Initial Value Problems in Ordinary Differential Equations*, Prentice-Hall, Inc., 1971.

[15] Cruise, D. R., "Notes on the Rapid Computation of Chemical Equilibrium", *Journal of Physical Chemistry*, Vol. 68, 1964, p. 3797.

[16] Lewis, M. J., "The Prediction of Inlet Flow Stratification and Its Influence on the Performance of Air-breathing Hypersonic Propulsion Systems", MIT Sc.D. Thesis, 1988.

[17] Chinitz, W., "Theoretical Studies of the Ignition and Combustion of Silane - Hydrogen-Air Mixtures", NASA-CR-3876, 1985.

[18] Jachimowski, C. J. and McLain, A. G., "A Chemial Kinetic Mechanism for the Ignition of Silane/ Hydrogen Mixtures", NASA-TP-2729, 1983.

[19] U.S. Dept. of Health and Human Services, *1980 Registry of Toxic Effects of Chemical Substances*, edited by Lewis, R. J. and Tatkin, Rodger L.

[20] Schick, Harold L., "A Thermodynamic Analysis of the High Temperature Vaporization Properties of Silica", *Chemical Reviews*,1960.

[21] Diskin, G. S. and Northam, B., "Effects of Scale on Supersonic Combustor Performance", AIAA Paper 87-2164.

Appendix A

Thermodynamic and Reaction Rate Data

Equilibrium Data

For individual species in thermal equilbrium, the enthalpy is a function of temperature alone. Several sources have developed polynomial curvefits for the enthalpy of many simple chemical species as a function of temperature. Given below are the coefficients used throughout this thesis for the calculation of enthalpy.

The curvefit for the enthalpy is:

$$\frac{H}{RT} = a_1 + \frac{a_2}{2}T + \frac{a_3}{3}T^2 + \frac{a_4}{4}T^3 + \frac{a_5}{5}T^4 + \frac{a_6}{T} \tag{A.1}$$

The curvefits may also be used to find the Gibb's free energy, G, of a chemical species:

$$\frac{G}{RT} = a_1(1 - \log(T)) - \frac{a_2}{2}T - \frac{a_3}{6}T^2 - \frac{a_4}{12}T^3 - \frac{a_5}{20}T^4 + \frac{a_6}{T} - a_7 \tag{A.2}$$

Tables A.1 and A.2 show the coefficients for the polynomials for the chemical species considered in this thesis.

Reaction Data

Table A.3 presents the hydrogen-air reaction mechanism. Included are the values of the constants in the Arrenhius expression of Equation (2.14).

Table A.4 lists the third body efficiency factors used for the H_2-air reaction (see Equation 2.18).

Table A.5 shows the additional reactions and Arrenhius constants used in the calculations involving silane.

Table A.1:
Polynomial curvefit coefficients for the enthalpy of individual chemical species in thermal equilibrium as a function of temperature .
For each species, the first set of coefficients is for $1000K < T < 5000K$. The second set is for $300K < T < 1000K$.

Species	a_1	a_2	a_3	a_4	a_5	a_6	a_7
AR	0.2500000E+01	0.0000000E+00	0.0000000E+00	0.0000000E+00	0.0000000E+00	-.7453750E+03	0.4366107E+01
	0.2500000E+01	0.0000000E+00	0.0000000E+00	0.0000000E+00	0.0000000E+00	-.7453750E+03	0.4366107E+01
CO	0.2951152E+01	0.1552557E-02	-.6191141E-06	0.1135034E-09	-.7788273E-14	-.1423183E+05	0.6531445E+01
	0.3787133E+01	-.2170953E-02	0.5075733E-05	-.3473773E-08	0.7721684E-12	-.1436351E+05	0.2633546E+01
CO_2	0.4412927E+01	0.3192289E-02	-.1297823E-05	0.2414745E-09	-.1674299E-13	-.4894404E+05	-.7287570E+00
	0.2171010E+01	0.1037811E-01	-.1073394E-04	0.6345918E-08	-.1628070E-11	-.4835260E+05	0.1066439E+02
H	0.2500000E+01	0.0000000E+00	0.0000000E+00	0.0000000E+00	0.0000000E+00	0.2547050E+05	-.4600109E+00
	0.2500000E+01	0.0000000E+00	0.0000000E+00	0.0000000E+00	0.0000000E+00	0.2547049E+05	-.4600109E+00
H_2	0.3043690E+01	0.6118711E-03	-.7399355E-08	-.2033191E-10	0.2459379E-14	-.8549100E+03	-.1648134E+01
	0.2846080E+01	0.4193211E-02	-.9611930E-05	0.9512260E-08	-.3309340E-11	-.9672530E+03	-.1411780E+01
H_2O	0.2670753E+01	0.3031712E-02	-.8535157E-06	0.1179085E-09	-.6197357E-14	-.2988899E+05	0.6883839E+01
	0.4156502E+01	-.1724433E-02	0.5698232E-05	-.4593004E-08	0.1423365E-11	-.3028877E+05	-.6861625E+00
HSiO	3.2708241E00	3.5195799E-03	-1.3772859E-06	2.4731356E-10	-1.6727435E-14	-2.614469E02	8.98612E00
	3.8647056E00	-5.3708648E-04	6.90345E-06	-6.6450605E-09	2.0576966E-12	-2.79054E02	6.57265E00
N	0.2442226E+01	0.1227619E-03	-.8499272E-07	0.2140083E-10	-.1251106E-14	0.5614882E+05	0.4492571E+01
	0.2514793E+01	-.1123379E-03	0.2964751E-06	-.3246405E-09	0.1259547E-12	0.5612777E+05	0.4119303E+01
N_2	0.2854576E+01	0.1597632E-02	-.6256625E-06	0.1131575E-09	-.7689707E-14	-.8901744E+03	0.6390288E+01
	0.3691615E+01	-.1333255E-02	0.2650310E-05	-.9768834E-09	-.9977220E-13	-.1062833E+04	0.2287498E+01
NO	0.3152936E+01	0.1405995E-02	-.5707846E-06	0.1062821E-09	-.7372078E-14	0.9852205E+04	0.6944646E+01
	0.4146947E+01	-.4119724E-02	0.9692247E-05	-.7863364E-08	0.2230951E-11	0.9744789E+04	0.2569429E+01

Table A.2:
Polynomial curvefit coefficients for the enthalpy of individual chemical species in thermal equilibrium as a function of temperature (con't).
For each species, the first set of coefficients is for $1000K < T < 5000K$. The second set is for $300K < T < 1000K$.

Species	a_1	a_2	a_3	a_4	a_5	a_6	a_7
O	0.2537257E+01	-.1842219E-04	-.8801792E-08	0.5964362E-11	-.5574361E-15	0.2923001E+05	0.4946794E+01
	0.3021889E+01	-.2173725E-02	0.3754220E-05	-.2994720E-08	0.9077755E-12	0.2913719E+05	0.2646008E+01
O_2	0.3597613E+01	0.7814560E-03	-.2238667E-06	0.4249016E-10	-.3346020E-14	-.1192792E+04	0.3749266E+01
	0.3718990E+01	-.2516720E-02	0.8583735E-05	-.8299870E-08	0.2708218E-11	-.1057670E+04	0.3908070E+01
OH	0.2889555E+01	0.9983506E-03	-.2187990E-06	0.1980278E-10	-.3845294E-15	0.3881179E+04	0.5559701E+01
	0.3823470E+01	-.1118723E-02	0.1246682E-05	-.2103590E-09	-.5254655E-13	0.3585279E+04	0.5825303E+00
SiH_2	2.2296977E00	4.7109215E-03	-1.7660321E-06	3.0648681E-10	-2.0167044E-14	2.8305E04	9.91442E00
	3.5513649E00	-2.506987E-03	1.2354987E-05	-1.1750895E-08	3.8124390E-12	2.8133E04	4.00301E00
SiH_3	2.8027662E00	6.2504497E-03	-2.2891516E-06	3.8993098E-10	-2.5275780E-14	2.2284E04	7.89061E00
	3.3995052	4.2678348E-03	2.0332684E-07	-1.1548308E-09	4.1288359E-13	2.1951E04	4.9103E00
SiH_4	4.2864439E+00	8.9421998E-03	-3.703074E-06	6.9171116E-10	-4.8137695E-14	1.9035952E+03	-3.1698731E+00
	1.6111312E00	1.2719990E-02	-1.6884339E-06	-4.5135745E-09	2.0400319E-12	2.9021544E+03	1.1738476E+01
SiH_2O	3.560942E00	5.69578E-03	-2.04376E-06	3.31588E-10	-2.00591E-14	-1.82842E04	3.90748
	4.42202e00	-7.11723e-03	3.0123e-5	-3.02044e-8	1.023143e-11	-1.78783e04	2.30345e00
SiO	3.7295164E+00	8.6335951E-04	-3.589447E-07	6.8212796E-11	-4.7844561E-15	-1.200831E+04	3.7472829E+00
	3.3495882E00	-2.6538250E-04	5.4814021E-06	-6.8793292E-09	2.6110821E-12	-1.1797081E04	6.2421835E00
SiO_2	6.0437403E00	1.6137498E-03	-7.0033700E-07	1.3480464E-10	-9.5718915E-15	-4.3344032E04	-7.9015665E00
	2.7328389E00	1.2359266E-02	-1.3902723E-05	7.3205169E-09	-1.4275135E-12	-4.2517933E04	8.7842538E00

Table A.3: Reaction mechanism for the H_2-Air system and values of the constants for the Arrenhius expression. The units of A are either $moles/(m^3 - sec)$ or $moles/(m^6 - sec)$; n is dimensionless; B is given in J/mole.

#	Reaction	A	n	B
H1	$H + O_2 \rightleftharpoons OH + O$	2.2×10^8	0.	70352.
H2	$H_2 + O \rightleftharpoons OH + H$	7.5×10^7	0.	46478.
H3	$OH + H_2 \rightleftharpoons H + H_2O$	2.0×10^7	0.	21633.
H4	$M + O + H_2O \rightleftharpoons 2OH + M$	5.85×10^7	0.	75377.
H5	$M + H_2 \rightleftharpoons 2H + M$	5.5×10^{12}	-1.0	432571.
H6	$M + H_2O \rightleftharpoons H + OH + M$	5.2×10^{15}	-1.5	494137.
H7	$H_2 + O_2 \rightleftharpoons 2OH$	1.0×10^7	0.	180067.
H8	$M + H + O_2 \rightleftharpoons HO_2 + M$	2.3×10^3	0.	-3350.
H9	$H + HO_2 \rightleftharpoons H_2 + O_2$	2.4×10^7	0.	2910.
H10	$OH + HO_2 \rightleftharpoons O_2 + H_2O$	3.0×10^7	0.	0.
H11	$M + O_2 \rightleftharpoons M + 2O$	7.2×10^{12}	-1.0	493752.
H12	$M + H + O \rightleftharpoons OH + M$	7.1×10^6	-1.0	0.
H13	$H_2 + O_2 \rightleftharpoons H_2O + O$	4.1×10^7	0.	211348.
H14	$H + NO \rightleftharpoons OH + N$	1.7×10^8	0.	203686.
H15	$O + NO \rightleftharpoons O_2 + N$	1.5×10^3	1.0	162117.
H16	$N_2 + O \rightleftharpoons NO + N$	5.0×10^7	0.	315422.
H17	$M + NO \rightleftharpoons O + N + M$	4.1×10^{12}	-1.0	626276.
H18	$H_2O_2 + M \rightleftharpoons 2OH + M$	1.2×10^{11}	0.	190381.
H19	$H_2 + HO_2 \rightleftharpoons H + H_2O_2$	7.3×10^5	0.	78148.
H20	$H + H_2O_2 \rightleftharpoons OH + H_2O$	3.2×10^8	0.	37449.
H21	$OH + HO_2 \rightleftharpoons O + H_2O_2$	5.2×10^4	0.5	88128.
H22	$H_2O + HO_2 \rightleftharpoons OH + H_2O_2$	2.8×10^6	0.	137179.
H23	$2HO_2 \rightleftharpoons H_2O_2 + O_2$	2.0×10^6	0.	0.

Table A.4: Third body efficiency factors for the H_2-air system.

Reaction #	Species	Efficiency Factor
H12	O_2	4.0
H12	O	10.0
H12	H_2O	2.0
H5	H	5.0
H5	H_2	2.0
H5	H_2O	8.0
H6	H_2O	6.0
H8	H_2	2.0
H8	H_2O	13.0

Table A.5: Silane reaction mechanism and values of the Arrenhius expression constants. The units on A are $moles/(m^3 - sec)$ or $moles/(m^6 - sec)$; n is dimensionless; B is given in J/mole.

#	Reaction	A	n	B
S1	$SiH_4 + M \rightleftharpoons SiH_3 + H + M$	2.0×10^5	0.	246862.
S2	$SiH_4 + SiH_3 \rightleftharpoons 2\,SiH_3 + H$	7.8×10^5	0.	29205.
S3	$SiH_4 + O_2 \rightleftharpoons SiH_2O + H_2O$	2.0×10^8	0.	82008.
S4	$SiH_4 + H \rightleftharpoons SiH_3 + H_2$	2.88×10^7	0.	11088.
S5	$SiH_4 + O \rightleftharpoons SiH_3 + OH$	4.1×10^6	0.	6611.
S6	$SiH_4 + OH \rightleftharpoons SiH_3 + H_2O$	8.6×10^6	0.	397.5
S7	$SiH_3 + O_2 \rightleftharpoons SiH_2O + OH$	1.7×10^8	0.	47824.
S8	$SiH_3 + O \rightleftharpoons SiH_2O + H$	1.3×10^8	0.	8368.
S9	$SiH_3 + OH \rightleftharpoons SiH_2O + H_2$	5.0×10^6	0.	0.
S10	$SiH_2O + M \rightleftharpoons HSiO + H + M$	5.0×10^4	0.	320502.
S11	$SiH_2O + H \rightleftharpoons HSiO + H_2$	3.3×10^8	0.	43933.
S12	$SiH_2O + O \rightleftharpoons HSiO + OH$	1.8×10^7	0.	12887.
S13	$SiH_2O + OH \rightleftharpoons HSiO + H_2O$	7.5×10^6	0.	711.3.
S14	$SiH_2O + O_2 \rightleftharpoons HSiO + HO_2$	3.95×10^8	0.	123431.
S15	$HSiO + M \rightleftharpoons SiO + H + M$	5.0×10^2	0.	121339.
S16	$HSiO + H \rightleftharpoons SiO + H_2$	2.0×10^8	0.	0.
S17	$HSiO + O \rightleftharpoons SiO + OH$	1.0×10^8	0.	0.
S18	$HSiO + OH \rightleftharpoons SiO + H_2O$	1.0×10^8	0.	0
S19	$HSiO + O_2 \rightleftharpoons SiO + HO_2$	1.2×10^8	0.	15879.
S20	$SiO + O_2 \rightleftharpoons SiO_2 + O$	1.0×10^7	0.	27197.
S21	$SiO + OH \rightleftharpoons SiO_2 + H$	4.0×10^6	0.	23849.
S22	$SiO + O + M \rightleftharpoons SiO_2 + M$	2.5×10^3	0.	18285.